JACS
JOURNAL OF THE AMERICAN CHEMICAL SOCIETY
Article
pubs.acs.org/JACS

The Mechanism of Efficient Asymmetric Transfer Hydrogenation of Acetophenone Using an Iron(II) Complex Containing an (*S*,*S*)-$Ph_2PCH_2CH{=}NCHPhCHPhN{=}CHCH_2PPh_2$ Ligand: Partial Ligand Reduction Is the Key

Alexandre A. Mikhailine, Mazharul I. Maishan, Alan J. Lough, and Robert H. Morris*

Davenport Laboratory, Department of Chemistry, University of Toronto, 80 St. George Street, Toronto, Ontario M5S 3H6, Canada

Supporting Information

ABSTRACT: On the basis of a kinetic study and other evidence, we propose a mechanism of activation and operation of a highly active system generated from the precatalyst *trans*-[Fe(CO)(Br)($Ph_2PCH_2CH{=}N$-((*S*,*S*)-C(Ph)H−C(Ph)H)-$N{=}CHCH_2PPh_2$)][BPh_4] (**2**) for the asymmetric transfer hydrogenation of acetophenone in basic isopropanol. An induction period for catalyst activation is observed before the catalytic production of 1-phenethanol. The activation step is proposed to involve a rapid reaction of **2** with excess base to give an ene−amido complex [Fe(CO)($Ph_2PCH_2CH{=}N$-((*S*,*S*)-C(Ph)H−C(Ph)H)-$NCH{=}CHPPh_2$)]$^+$ ($\mathbf{Fe_p}$) and a bis(enamido) complex Fe(CO)($Ph_2PCH{=}CH$-*N*-(*S*,*S*-CH-(Ph)CH(Ph))-$N{-}CH{=}CHPPh_2$) (**5**); **5** was partially characterized. The slow step in the catalyst activation is thought to be the reaction of $\mathbf{Fe_p}$ with isopropoxide to give the catalytically active amido-(ene-amido) complex $\mathbf{Fe_a}$ with a half-reduced, deprotonated PNNP ligand. This can be trapped by reaction with HCl in ether to give, after isolation with $NaBPh_4$, [Fe(CO)(Cl)($Ph_2PCH_2CH_2N$(H)-((*S*,*S*)-CH(Ph)CH(Ph))-$N{=}CHCH_2PPh_2$)][BPh_4] (**7**) which was characterized using multinuclear NMR and high-resolution mass spectrometry. When compound **7** is treated with base, it directly enters the catalytic cycle with no induction period. A precatalyst with the fully reduced P-NH-NH-P ligand was prepared and characterized by single crystal X-ray diffraction. It was found to be much less active than **2** or **7**. Reaction profiles obtained by varying the initial concentrations of acetophenone, precatalyst, base, and acetone and by varying the temperature were fit to the kinetic model corresponding to the proposed mechanism by numerical simulation to obtain a unique set of rate constants and thermodynamic parameters.

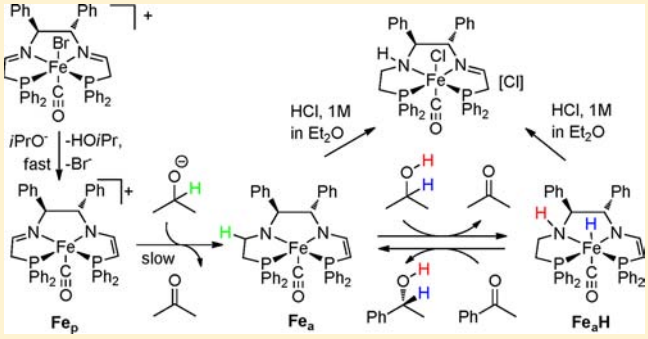

INTRODUCTION

The asymmetric reduction of polar unsaturated bonds allows the production of valuable chiral secondary alcohols and amines for use as chiral building blocks in industry and academia. Classical methods for the synthesis of such products involve the use of a reagent from the chiral pool or the resolution of a mixture of enantiomers. Both of these have the following drawbacks: the use of expensive reagents, the generation of waste, and costly workup. Asymmetric catalytic reductions utilizing transition metals,[1] enzymes,[2] organocatalysts,[3] and other metal-free compounds[4] are being developed to offer cheaper and more environmentally friendly alternatives.[5]

The complexes containing platinum group metals (such as Ru, Rh, and Ir) and chiral ligands are especially active and have been developed to be highly enantioselective.[1a,c,6] The information gained from mechanistic studies[7] on these catalytic systems greatly assists in the optimization and scaling up of the process for industrial application.[5a,c,6c] Nevertheless, there are some negative features of these catalytic systems such as the high price, low availability and high toxicity of the metal that make them undesirable for some applications. Recent developments to overcome these drawbacks involve the use of first-row transition metals for asymmetric catalysis. Low-valent iron is an especially attractive candidate for this role, since it is cheap, abundant, and nontoxic compared to ruthenium. Iron-containing catalysts for asymmetric reduction reactions are proving to be promising.[8] Highly reactive and selective catalytic systems for the direct[9] and transfer hydrogenation[10] of ketones and recently ketimines[11] using iron have now been developed. On the other hand, there are only a few studies of their mechanism of action.[9c,12]

Complex **1** (Figure 1) was the first fully characterized iron-based precatalyst for the effective asymmetric transfer hydrogenation (ATH) of aromatic ketones.[9b,13] A second generation of catalyst (**2**) was designed with a ligand that maintained the key phosphorus and nitrogen chelates, which are known to be important for bifunctional catalysis. Although the resulting

Received: May 24, 2012
Published: July 13, 2012

   dx.doi.org/10.1021/ja304814s | *J. Am. Chem. Soc.* 2012, 134, 12266−12280

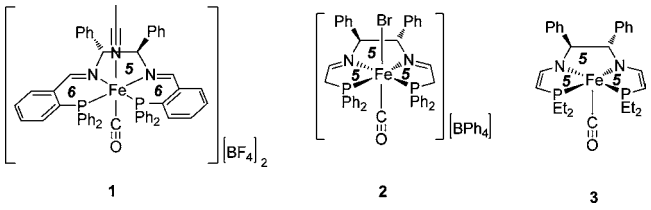

1 2 3

Figure 1. Structures of highly active iron(II)-based precatalysts for the ATH of aromatic ketones.

structure was found to be distorted from an octahedral geometry, the precatalyst **2** showed exceptionally high activity and enantioselectivity in the catalytic reduction of ketones.[14] The effect on the catalyst activity by changing substituents on the ligand was also explored, a task that was relatively straightforward due to the ease of the template synthesis of the complexes.[15] A variation of the substituents at the phosphorus atom showed that only a narrow range of structures result in active catalysts; the effective substituents were ethyl, phenyl, or aryl groups substituted with methyl groups in the meta or para positions.[16] Bulky substituents at phosphorus such as cyclohexyl, isopropyl, or *o*-tolyl prevented catalysis. This is evidence against mechanisms that require the breaking of an iron−phosphorus bond such as a Meerwein−Ponndorf−Verley mechanism.[16b] A study of the use of different diamines serving as the backbone of the ligand demonstrated that the (*R*,*R*)- or (*S*,*S*)-stilbenyl (CHPhCHPh) backbone gave optimum activity and enantioselectivity in the ATH of acetophenone, while surprisingly, the ethylene backbone gave a reduced activity.[17]

The ligands of precatalysts **1** and **2** are constructed from different phosphino-aldehyde precursors. The smaller phosphino-aldehyde used for **2** results in a PNNP ligand that forms smaller ring sizes with the metal (5,5,5 in **2** vs 6,5,6 in **1**) and a wider P−Fe−P angle.[15a] The most interesting difference, on the other hand, is associated with the presence of the acidic β-hydrogens in ligand of **2**. Recently, our group discovered that dicationic complexes, identical to **2** but with electron-donating substituents on phosphorus, undergo double deprotonation when reacted with base in nonpolar solvents to give neutral ene−amido iron complexes, for example, complex **3** (Figure 1).[18] The neutral complex **3**, without preactivation by base, showed good activity in the catalytic reduction of acetophenone. The role in catalysis of such an ene−amido complex formed from **2** will be reported here.

Ruthenium complexes containing tetradentate ligands with two phosphorus and two nitrogen donors have been used in a variety of catalytic transformations[19] including the catalytic asymmetric reductions of ketones.[20] Interestingly enough, transfer hydrogenation with the catalysts bearing P-N(H)-N(H)-P ligands are much more active due to their ability to form amido−metal species after activation with base, compared to the complexes with imine PNNP ligands.[7a] By contrast iron-based catalysts for the asymmetric reduction of aromatic ketones, including complexes **1** and **2**, do not follow this rule, since they contain PNNP ligands with imine functionalities.[9b,14] It is important in the current study to determine whether the ligand on iron can be reduced under the catalytic conditions to the diamine ligand. The reduction of ketones could then proceed according to the bifunctional outer-sphere mechanism similar to that observed for the ruthenium-based complexes where a metal−hydride and an amine proton attack the ketone in the carbonyl reduction step.

Here we describe a study of the mechanism of action of a catalyst system that is highly active and selective for the ATH of ketones. It is based on precatalyst **2** (Figure 1) which has iron(II) coordinated by a PNNP ligand.

RESULTS

Kinetics of the Process. The catalytic reduction of acetophenone to 1-phenethanol was chosen for study because it is the standard reaction used to test ATH catalysts. The optimized conditions for the ATH of acetophenone to produce enantioenriched 1-phenethanol using *i*PrOH as a solvent and a reducing agent were previously reported by our group and are summarized in Scheme 1.[17] The iron precatalyst **2** was

Scheme 1. General Reaction of the Catalytic Reduction of Acetophenone

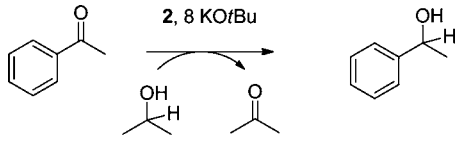

Conditions:	
[Catalyst]	1.53×10^{-5} - 1.07×10^{-4} M
[Substrate]	0.263 - 0.662 M
[Acetone]	0 - 0.164 M
[KO*t*Bu]	1.35×10^{-3} - 4.08×10^{-4} M
[*i*PrOH]	12.4 M
Temperature	19-41 °C

synthesized by a template reaction followed by substitution with carbon monoxide.[17] A strong base such as KO*t*Bu is required for the activation of the catalyst and is used in 8-fold excess relative to the catalyst.

Reaction Profile. The reaction profile shown in Figure 2 (the run at standard conditions) was previously reported and was obtained by monitoring the formation of the product as a function of time. The reaction consists of three stages: initiation (increasing rate of the reaction), maximum rate of the reaction

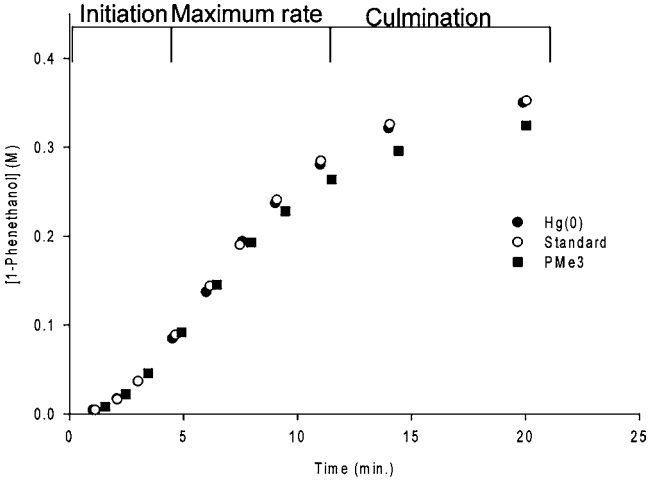

Figure 2. Effect of the addition of Hg(0) and substoichiometric amounts of trimethylphosphine on the reaction rate of the transfer hydrogenation of acetophenone (Hg(0) was added at 6.9 min, and PMe_3 at 6.5 min, after reaction was initiated).

dx.doi.org/10.1021/ja304814s | J. Am. Chem. Soc. 2012, 134, 12266−12280

(a linear region), and culmination (decreasing rate of the reaction).

A prolonged induction period is not common in homogeneous catalysis, since the activation of the catalyst is usually a fast process. However, induction periods for activation have been observed, for example, for phosphine rhodium(I), iridium(I),[21] and arene ruthenium(II)[22] complexes. Such an induction period might also indicate the formation of soluble or insoluble metal particles and/or nanoparticles that serve as heterogeneous catalysts.[23] This induction process, explained by Finke and co-workers,[24] has two steps for particle formation, first slow nucleation and then fast agglomeration.

The observed sigmoidal kinetics of our system forced us to explore the true nature of the catalytic species. One of the most commonly reported methods in the literature for differentiating between hetero- and homogeneous catalysts is the mercury test.[25,26] It is based on the property of metals to form an amalgam with Hg(0). Therefore, if mercury is added to the catalytic mixture, it should deactivate a heterogeneous catalyst but not affect the activity of a homogeneous catalyst. This test can be efficiently applied to the Pt, Pd, and Ni metals that form an amalgam with elemental mercury.[26] On the other hand, this test can be misleading when applied to the catalytic systems that are based on Ir, Rh, Ru, and Fe because they may not form an amalgam with Hg(0). Nevertheless, examples of successful quenching of the heterogeneous catalysis using Hg(0), for example with rhodium complexes, are known.[27] Even though our system is based on iron, this test was applied by adding 300 equiv of mercury to the reaction mixture containing initially **2**, acetophenone, KO*t*Bu, and *i*PrOH at 28.0 °C in an argon glovebox after 6.90 min of reaction (Figure 2, Hg(0)). The reaction progression was unaffected by the addition. Thus, either the catalyst is homogeneous, or catalytic Fe particles were not deactivated by Hg(0).[28] The inconclusive outcome of the Hg(0) test forced us to perform additional testing.

A "fractional poisoning" experiment is rarely reported in the literature but can be a powerful technique to differentiate between hetero- and homogeneous catalysis.[13b,25,29] The reasoning behind this test is that metal particles have only a fraction of the active metal on the surface of the particle to perform catalysis. Therefore, a heterogeneous catalyst can be poisoned with less than one equivalent of the quenching agent relative to the catalyst, compared to the homogeneous catalyst that would usually require one equivalent of poisoning agent for the quenching or more than one if reversible inhibition is taking place. Trimethylphosphine was chosen to be a poisoning agent for our system, since it binds strongly to low-valent metals and is not a sterically demanding ligand. This additive poisons our first-generation catalysts which are thought to form active iron nanoparticles.[13b] The test was conducted using the same conditions as were used for the Hg(0) poisoning experiment except 0.5 equiv of PMe_3 relative to the catalyst was added at 6.5 min of reaction time (Figure 2, PMe_3). The reaction slowed a little but was not poisoned completely. This observation supports the proposal that the active catalytic species are sterically hindered homogeneous complexes and not surface atoms of nanoparticles. The reproducibility of the kinetics and the high enantioselectivity of the process also argue for a homogeneous process. Finally, we will show below that a well-defined complex can be isolated that serves as an extremely active catalyst without the induction period.

When a high loading of the substrate (6000 equiv relative to the catalyst) is used, the turnover frequency of the process decreases after 60% of the acetophenone is converted to the corresponding alcohol. The decomposition of the catalyst is not the cause of this slowdown because the addition of substrate to the reaction mixture after 60% conversion increases the rate of reaction to the expected value.[17] Instead it appears that the slower rate results from the system approaching equilibrium. Whether a high (0.1%) or low (0.01%) catalyst loading is employed, the reaction attains about 88% conversion at 28.0 °C. This corresponds to an equilibrium constant K_{eq} of 0.24 (eq 1).

$$K_{eq} = \frac{[\text{acetone}]_{eq}[\text{phenethanol}]_{eq}}{[i\text{PrOH}]_{eq}[\text{acetophenone}]_{eq}} = 0.24 \pm 0.02 \quad (1)$$

Maximum Rate Determination and Analysis. A systematic variation of the reaction conditions was conducted in an attempt to determine rate laws for the catalyst activation and 1-phenethanol formation. The kinetics method of measuring initial rates cannot be used to explore the mechanism of this reaction because of the induction period. However, a constant, maximum rate of 1-phenethanol production is observed in the region between approximately 10 and 60% conversion (Figure 2 and 3), and the variation in this rate with changes in the concentrations of the reagents provides useful information. The process of precatalyst activation cannot be monitored directly, since the concentrations of active species are very difficult to measure accurately. For that reason, we used the intercept of the 1-phenethanol formation line with the time axes (Figure 3). The intercept is a measure of the time required for the precatalyst to be activated in order to produce the maximum rate of catalysis.

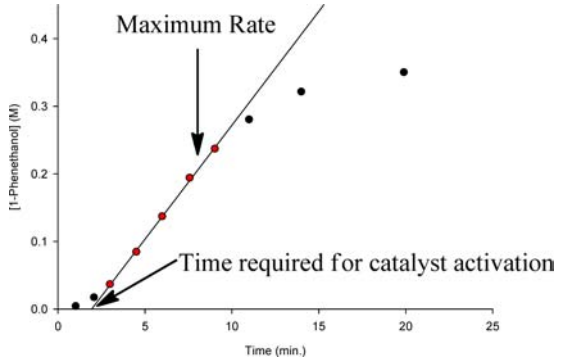

Figure 3. Plot showing how the maximum rate and activation period were determined.

To ensure the reproducibility of results, the catalytic reductions of acetophenone were conducted at 28.0 ± 0.3 °C in an argon glovebox using the following standard concentrations of reagents, which were achieved using a series of dilutions, unless otherwise stated: the concentrations of acetophenone, **2**, KO*t*Bu, and *i*PrOH were 0.412, 6.73×10^{-5}, 5.45×10^{-4}, and 12.4 M, respectively (detailed procedures, initial concentration, and experimental results can be found in the Supporting Information). The reactions were initiated by addition of the base solution to a mixture containing **2**, *i*PrOH, and acetophenone.

A plot of the maximum rate of 1-phenethanol formation versus the precatalyst concentration is nonlinear (Figure 4a). Nevertheless, it can be seen that the rate is positively dependent on the precatalyst concentration. The time required for the

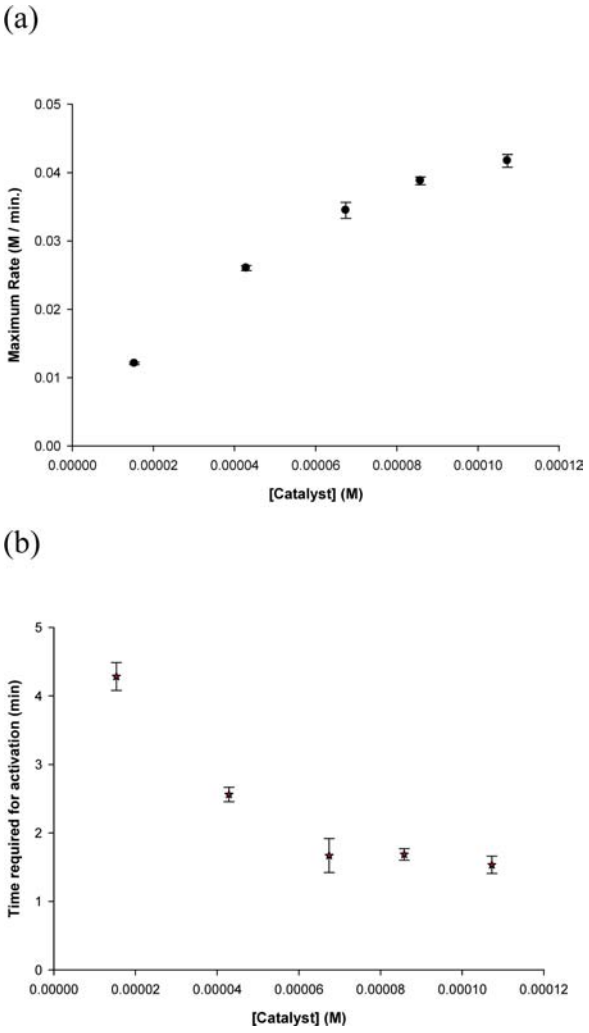

Figure 4. Plots of (a) the maximum rate of 1-phenethanol formation versus the precatalyst concentration and (b) the time for catalyst activation versus the precatalyst concentration. Conditions: [acetophenone] = 0.412 M; [**2**] = 1.07× 10^{-4}, 8.58 × 10^{-5}, 6.74 × 10^{-5}, 4.29 × 10^{-5}, 1.53 × 10^{-5} M; [KO*t*Bu] = 5.45 × 10^{-4} M, [*i*PrOH] = 12.4 M; temperature 28 °C.

activation of the catalyst is inversely proportional to the concentration of **2** (Figure 4b), when its concentration is significantly lower than the base concentration (below 7 × 10^{-5} M). At higher concentrations the activation step becomes almost independent of the concentration of **2**. This can be attributed to the fact that the number of equivalents of the precatalyst relative to the base is greater than a 1:5; thus, the base becomes a rate-limiting reagent.

Attempts were made to activate the catalyst before the addition of the ketone. Initially, we reacted the catalyst with the base for 12 min followed by the addition of substrate and obtained a complete shutdown of reactivity. An approximately one minute reduction in the activation period compared to the standard run was observed when the catalyst was reacted with the base for 2 min prior to the addition of the ketone and showed activity comparable to that of the standard run. The color of solutions in both experiments changed from yellow to green instantaneously after the addition of the base. The color of the reaction mixture gradually changed to a yellow-brown over the course of 12 min. These observations indicate that the formation of the active catalyst by the reaction of the precatalyst and basic *i*PrOH is the cause of the induction period and that the active species decomposes in the presence of excess of base, when the ketone is not part of the reaction mixture.

There is a positive dependence of the maximum rate on acetophenone concentration (Figure 5a). Figure 5b shows that increasing the concentration of acetophenone causes a decrease in the rate of the precatalyst activation.

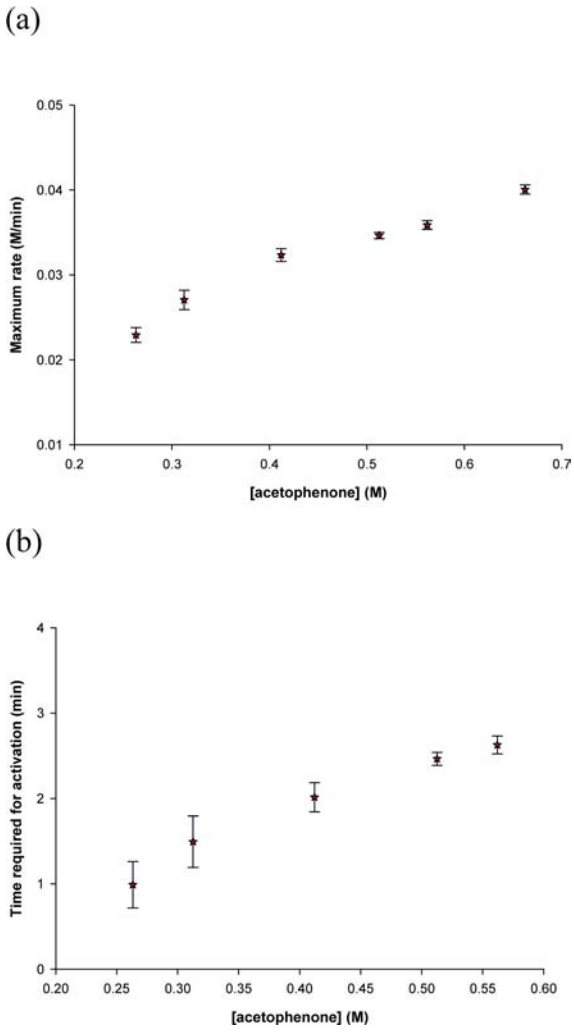

Figure 5. (a) Dependence of maximum rate of 1-phenethanol formation on the acetophenone concentration. (b) Dependence of the time required for the precatalyst to be activated on the acetophenone concentration. Conditions: [acetophenone] = 0.263, 0.313, 0.412, 0.513, 0.562, 0.662 M; [**2**] = 6.74 × 10^{-5} M; [KO*t*Bu] = 5.45 × 10^{-4} M, [*i*PrOH] = 12.4 M; temperature 28 °C.

The interference by acetophenone on the activation of the catalyst is an unexpected outcome; ketones are poor ligands and are unlikely to prevent the isopropoxide from coordinating to the iron and activating the catalyst. On the other hand, the enolate form of acetophenone, which can be easily formed under the experimental conditions,[30] would be a much better ligand. Support for inhibition by the enolate comes from a previously reported experiment where benzophenone, a nonenolizable ketone, was found to have no effect on the reaction rate.[16b]

dx.doi.org/10.1021/ja304814s | *J. Am. Chem. Soc.* 2012, 134, 12266−12280

During the course of the reaction another ketone, acetone, is produced as a byproduct, and this, in its enolate form, may also interfere with the catalyst activation. Figure 6 verifies the fact that acetone has a weak inhibitory effect on the activation.

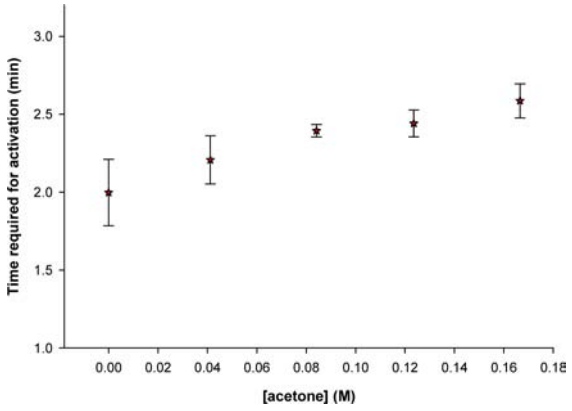

Figure 6. Dependence of the catalyst activation time on acetone concentration. Conditions: [acetophenone] = 0.412 M; [**2**] = 6.74×10^{-5} M; [KO*t*Bu] = 5.45×10^{-4} M, [*i*PrOH] = 12.4 M; [acetone] = 4.12×10^{-2}, 8.42×10^{-2}, 1.24×10^{-1}, 1.64×10^{-1} M; temperature 28 °C.

In our previous studies,[14] different bases such as NaO*i*Pr, KOH, and NaO*t*Bu were tested as activating agents for this process. The variation had a minor effect on the rate of the reaction, and it was concluded that neither the base nor its cation (Na^+ or K^+) participate in the actual catalytic cycle and only play an active role during the activation of the catalyst. Indeed, the data of Figure 7a show that the maximum rate is independent of the base (KO*t*Bu) concentration as long as it is at least 6 times greater than that of the catalyst. The experiments with less than 6 equiv of base per iron complex showed slower maximum rates because the activation of the catalyst took a longer time than the time for the reaction to go to completion. The dependence of the precatalyst activation time on the base concentration showed the expected inverse dependence (Figure 7 b). These observations are in agreement with our previous conclusions that the base is only important for the activation of the catalyst.

The attempts to investigate the dependence of the maximum rate on *i*PrOH concentration were not successful. We searched for a suitable solvent that was inert, weakly coordinating, and having a dielectric constant similar to that of *i*PrOH. When mixtures of THF and *i*PrOH or benzene and *i*PrOH were used, the rates were much lower than those expected on the basis of the standard runs. These observations show that the polarity and protic nature of the solvent are important factors in this catalytic reaction.

The Kinetic Model. The kinetic studies indicate that the catalyst activation is directly proportional to the precatalyst and the base concentrations. It is also inversely proportional to the concentration of the substrate (S) and acetone (A). These findings are schematically represented in Scheme 2. The nonactivated iron complex ($\mathbf{Fe_p}$) participates in an irreversible reaction with isopropoxide ($i\mathrm{PrO}^-$) to give catalytically active complexes ($\mathrm{Fe_{Ta}}$) (eq 2) and in two quickly established equilibria with the enolate of acetone (A^e) (eq 3) and the enolate of acetophenone (S^e) (eq 4) to give nonproductive iron-enolate species (Fe-A^e and Fe-S^e). Note that $\mathbf{Fe_p}$ may also reversibly react with base to give other species (for example complex **5**, see further for details) but these equilibria were not accounted for in the model since the concentrations of base and isopropanol stay approximately constant throughout the reaction, compared to the varying concentrations of acetone and acetophenone. The formation of the enolates A^e and S^e are

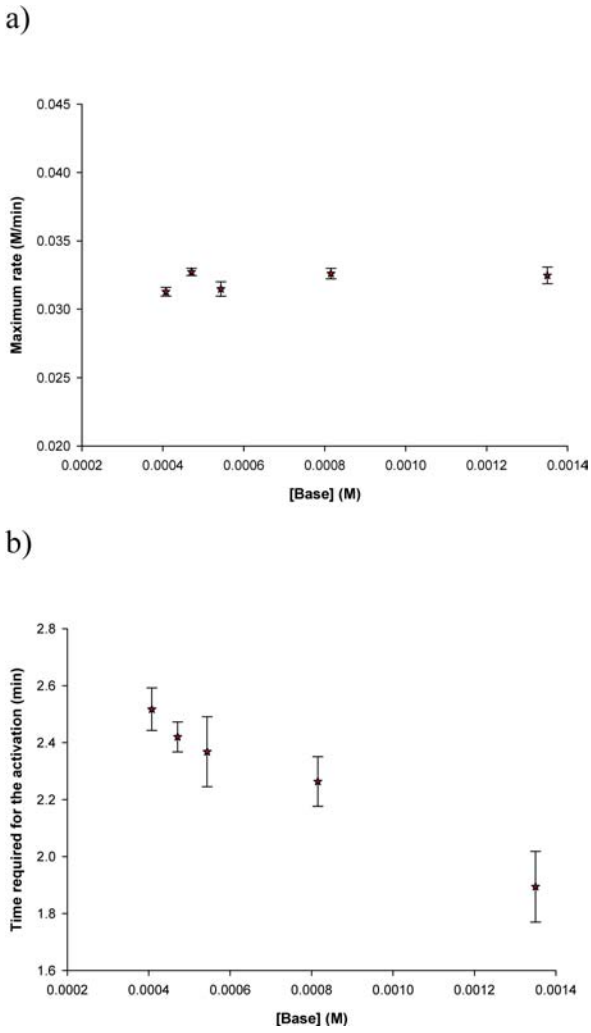

Figure 7. (a) Dependence of maximum rate of 1-phenethanol formation on the base concentration. (b) Dependence of catalyst activation time on the base concentration. Conditions: [acetophenone] = 0.413 M; [**2**] = 6.74×10^{-5} M; [KO*t*Bu] = 4.08×10^{-4}, 4.71×10^{-4}, 5.44×10^{-4}, 8.16×10^{-4}, 1.35×10^{-3} M, [*i*PrOH] = 12.4 M; temperature 28 °C.

Scheme 2. Schematic Representation of the Activation of Catalyst

$$\mathrm{Fe_p} + i\mathrm{PrO}^- \xrightarrow{k_{act}} \mathrm{Fe_{Ta}} \qquad \text{eq (2)}$$

$$\mathrm{A}^e + \mathrm{Fe_p} \underset{}{\overset{K_{1\_eq}}{\rightleftharpoons}} \mathrm{Fe\text{-}A}^e \qquad \text{eq (3)}$$

$$\mathrm{S}^e + \mathrm{Fe_p} \underset{}{\overset{K_{2\_eq}}{\rightleftharpoons}} \mathrm{Fe\text{-}S}^e \qquad \text{eq (4)}$$

$$\mathrm{A} + i\mathrm{PrO}^- \overset{K_{3\_eq}}{\rightleftharpoons} i\mathrm{PrOH} + \mathrm{A}^e \qquad \text{eq (5)}$$

$$\mathrm{S} + i\mathrm{PrO}^- \overset{K_{4\_eq}}{\rightleftharpoons} i\mathrm{PrOH} + \mathrm{S}^e \qquad \text{eq (6)}$$

dx.doi.org/10.1021/ja304814s | *J. Am. Chem. Soc.* 2012, 134, 12266−12280

described in terms of rapidly established equilibria with base and acetone (eq 5) or base and acetophenone (eq 6), respectively.

The rate of formation of Fe_{Ta} can be represented in terms of the concentrations of **2** ($[Fe_p]_0$), Fe_{Ta}, iPrO$^-$, A, and S and described by eq 7 (See Supporting Information for derivation).

$$\frac{d[Fe_{Ta}]}{dt} = \frac{k_{act}\{[Fe_p]_0 - [Fe_{Ta}]\} \times [iPrO^-]}{\left(1 + \frac{[iPrO^-]}{[iPrOH]} \times (K_{1.eq}K_{3.eq}[A] + K_{2.eq}K_{4.eq}[S])\right)} \quad (7)$$

The rate of 1-phenethanol formation depends on the concentrations of activated catalyst, substrate and possibly the hydrogen source, iPrOH. Similar dependences were previously observed by Adolfsson and co-workers for the ruthenium-based catalytic system containing pseudodipeptide ligands for the asymmetric transfer hydrogenation of acetophenone,[31] and thus this model can be applied to our catalytic process. The reduction can be represented in terms of two dependent equilibria (Scheme 3): an iron-containing active complex (**Fe$_a$**)

Scheme 3. Schematic Representation of the Hydrogen Transfer Process

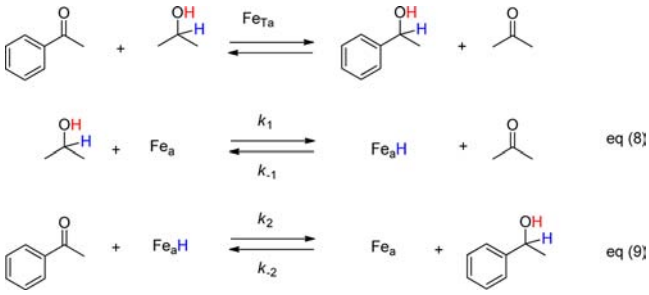

reacts with iPrOH (R) to give a complex with activated hydrogen or hydride (**Fe$_a$H**) and acetone (eq 8) and reaction of Fe$_a$H with acetophenone (S) to give 1-phenethanol and regenerate **Fe$_a$** (eq 9). The total concentration of active iron species $[Fe_{Ta}]$ is equal to $[\mathbf{Fe_a}] + [\mathbf{Fe_aH}]$.

Adolfsson and co-workers in their kinetic study assumed that the formation of the active ruthenium complex from the precatalyst is an instantaneous process; thus, the concentration of the precatalyst is equal to the concentration of the active species.[31] This assumption in combination with the derived rate law allowed the determination of all of the rate constants from the kinetic data. Unfortunately, in our iron-catalyzed reaction this assumption is not valid and $[\mathbf{Fe_p}] \neq [Fe_{Ta}]$. Moreover, $[Fe_{Ta}]$ is changing throughout the catalytic reaction and depends on the initial concentrations of the reagents.

The Simulation of the Rate Processes. In order to verify the legitimacy of the proposed kinetic model and estimate rate constants associated with it, numerical simulations were used. A change in concentration of every component of the reaction mixture in small intervals of time (Δt = 0.00025 s) can be determined from the equations which arise directly from the kinetic model (Schemes 2 and 3); these equations are given in the Supporting Information (eqs S18−S28). The concentrations of base and iPrOH are assumed to be constant during the reaction, since they are used in large excess compared to the other reagents, and are assumed to be equal to their initial concentrations.

The experimental data consisting of 18 catalytic runs (180 data points) conducted with various initial concentrations of precatalyst, acetophenone, acetone, and base were globally fitted by numerical simulation to determine an optimized, consistent set of the rate constants (Table 1). The plots showing both the experimental and fitted data points are presented in Figure 8.

Table 1. Estimated Rate Constants at 301 K from Simulated Reaction Profiles Using the Proposed Model (the error is less than 10%)

rate constants	(M^{-1} min^{-1})
k_1	6.5×10^2
k_{-1}	2.7×10^4
k_2	1.4×10^4
k_{-2}	1.4×10^3
k_{act}	2.7×10^2
$K_{1\_eq}K_{3\_eq} = K_{2\_eq}K_{4\_eq}$	1.2×10^5

The simulated reaction profiles are in good agreement with the experimental data points. A slight deviation between the simulated and the experimental data can be seen in Figure 8C with the lowest concentration of catalyst. Slower formation of 1-phenethanol can be explained by possible decomposition of the catalyst, which only becomes evident at low catalyst loadings (1.53×10^{-5} M); this was not taken into account in the simulation. Figure 8E shows the simulated concentrations of the iron precatalyst (**Fe$_p$** in Scheme 2), and the active iron species with and without a hydride equivalent (**Fe$_a$H** and **Fe$_a$** in Scheme 3, respectively) during the reaction with standard initial concentrations. From the plot it is evident that the active species have similar concentrations during the initiation and propagation segments of the reaction, but at equilibrium the active species without the hydride is predominant. Clearly, the formation of the active species is a continuous process that takes place with a diminishing rate over the course of the entire reaction.

Temperature Dependence. Catalytic reductions were conducted at various temperatures between 293.2 to 315.1 K in order to obtain corresponding reaction profiles. The maximum rates of these reactions result from the combined effects of different rate constants, and therefore cannot be used to determine the activation parameters of the rate-limiting step of the reaction. The rates constants of individual steps can be estimated by numerical simulations of the reaction profiles in a similar fashion to that done for the determination of rate constants, except that various K_{eq} values, which were experimentally determined, were used to determine the rate of the k_{-2} step (see eq S22 in Supporting Information). The simulated profiles along with the experimental data are presented in Figure 9. Five sets of rate constants that were used in the simulations of temperature variation reaction profiles are summarized in Table 2. These values were used to determine activation parameters of individual steps (Table 2) of the reaction using Eyring−Polanyi plots (Supporting Information).

The Gibbs free energies of activation of all of the steps of the process are relatively low. This is consistent with the observed high rate of the process. The activation energies of the catalytic steps are in a similar range, thus allowing the system to be driven by the thermodynamic equilibrium of the process. The highest energy point in the catalytic cycle is the reaction of

dx.doi.org/10.1021/ja304814s | J. Am. Chem. Soc. 2012, 134, 12266−12280

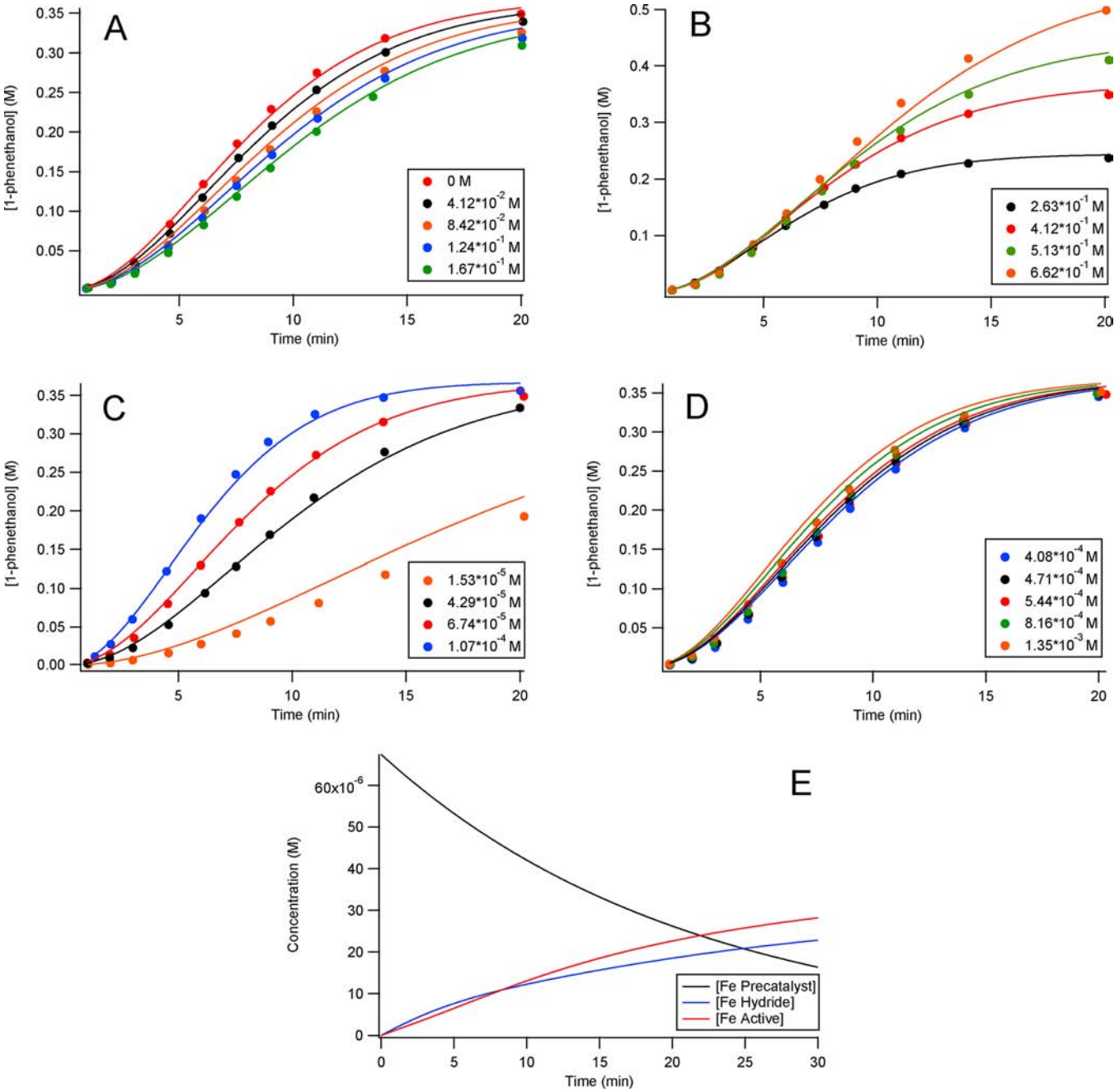

Figure 8. Experimental and simulated reaction profiles using the proposed model. Solid lines represent simulated reaction profiles. Plots A, B, C, and D represent experiments with various concentrations of acetone, acetophenone, precatalyst, and base, respectively. The initial concentrations of other reagents were kept constant and are equal to the standard concentrations. Plot E shows simulated concentrations of iron species in the reaction mixture as a function of time (simulated for the standard conditions: concentrations of acetophenone, **2**, base, and *i*PrOH were 0.412, 6.73×10^{-5}, 5.45×10^{-4}, and 12.4 M, respectively).

acetophenone with the $\mathbf{Fe_aH}$, although the free energy that is required to get to this transition state is smaller than the energy needed to activate $\mathbf{Fe_p}$ by reaction with *i*PrOH (16.7 kcal/mol) and the energy of the reaction of $\mathbf{Fe_a}$ with *i*PrOH (Figure 10).

The rates of individual steps at seven minutes of reaction time can be approximated by multiplying corresponding rate constants by the concentrations of reagents participating in particular step of the reaction at a given time. The concentrations of the reagents were determined from the experimental and simulated reaction profile of the standard run and are summarized in Table 2. The rates of forward reactions, which correspond to k_1 and k_2 (eqs 8 and 9) were faster compared to the reverse reactions, which correspond to k_{-1} and k_{-2}. The rate of forward reaction described by eq 8 was found to be almost twice as fast as the rate of the forward reaction described by the eq 9. This observation allows us to assume that at a given set of conditions the step involving the reduction of acetophenone is a rate-determining event in the catalytic cycle. Our previous studies also showed that the rate of reaction is highly dependent on the nature of the ketone used.[14] This supports the idea that the reaction of Fe_aH with the ketone is the rate-determining step under experimental conditions. On the other hand, it is possible that the reaction of *i*PrOH with

dx.doi.org/10.1021/ja304814s | J. Am. Chem. Soc. 2012, 134, 12266−12280

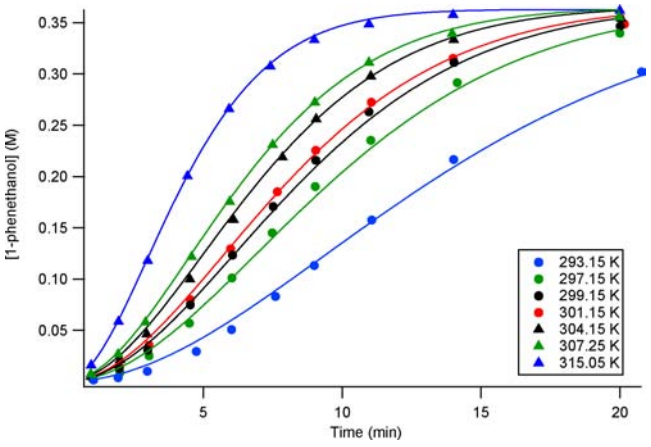

Figure 9. Experimental and simulated reaction profiles of temperature dependence experiments. Solid lines represent simulated reaction profiles. Conditions: [acetophenone] = 0.412 M; [**2**] = 6.74×10^{-5} M; [KO*t*Bu] = 5.45×10^{-4} M, [*i*PrOH] = 12.4 M; temperature 293.2, 297.2, 299.2, 301.2, 304.2, 307.3, 315.1 K.

Fe_a can be a rate-determining step when the concentration of acetophenone is high or the concentration of *i*PrOH is low.

The free energy for the process of converting 2-PrOH and acetophenone to acetone and 1-phenethanol can be independently determined from the equilibrium constant (eq 1) and from the activation parameters, which were obtained from simulations (Table 2 and Figure 10). The values 0.8 and 0.83 kcal/mol can be obtained, respectively. A good correspondence between the values further suggests that the proposed mechanistic model effectively describes the catalytic process under investigation.

Kinetic Isotope Effect. The kinetic isotope effect (KIE), as a ratio of the rates of hydrogen and deuterium transfer, was determined for the standard catalytic reductions that were conducted at constant temperatures using different hydrogen/deuterium donor sources: $(CH_3)_2C(H)OH$, $(CD_3)_2C(D)OD$, and $(CH_3)_2C(H)OD$. The formation of 1-phenethanol with respect to time is plotted in Figure 11. The resulting rates, which were determined at 29 °C, were used to calculate the KIE (Chart 1).

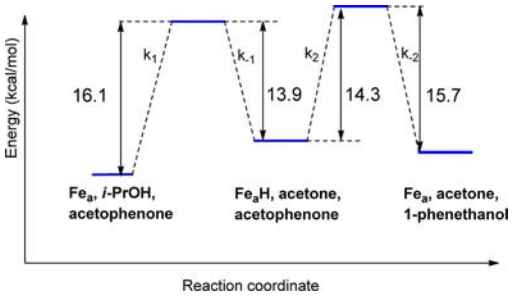

Figure 10. Reaction coordinate diagram for the catalytic step of the process.

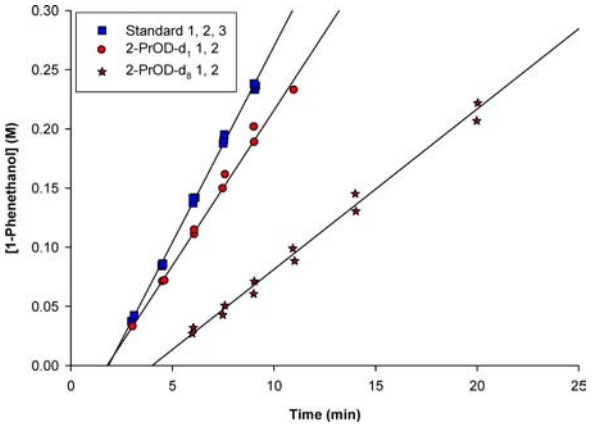

Figure 11. Rates of ATH of acetophenone using *i*PrOH deuterated at different positions.

Chart 1. Calculation of the Kinetic Isotope Effects Using $(CD_3)_2C(D)OD$ (KIE_1) and $(CH_3)_2C(H)OD$ (KIE_2)

$$KIE_1 = \frac{k_{obs}[(CH_3)_2C(H)OH]}{k_{obs}[(CD_3)_2C(D)OD]} = 2.5 \pm 0.1$$

$$KIE_2 = \frac{k_{obs}[(CH_3)_2C(H)OH]}{k_{obs}[(CH_3)_2C(H)OD]} = 1.3 \pm 0.1$$

A primary kinetic isotope effect (KIE_1 = 2.5) was observed when fully deuterated *i*PrOD was used, and a smaller kinetic

Table 2. Estimated Rate Constants of the Process at Different Temperatures and the Calculated Activation Parameters of Individual Steps of the Reaction[a]

temp	$k_{act} \times 10^2$	$k_1 \times 10^2$	$k_{-1} \times 10^4$	$k_2 \times 10^4$	$k_{-2} \times 10^3$	K_{eq}
293.2	1.43	4.61	2.10	1.01	0.830	0.256
297.2	2.15	5.81	2.24	1.17	1.23	0.248
299.2	2.48	6.26	2.42	1.32	1.40	0.244
301.2	2.74	6.48	2.72	1.36	1.36	0.240
304.2	3.25	6.95	3.17	1.59	1.49	0.234
307.3	3.68	7.80	3.56	1.64	1.58	0.228
315.1	6.19	10.4	4.76	2.19	2.27	0.212
rate[b]		0.078	0.036	0.035	0.002	
$\Delta H^{\ddagger}$	11.0	5.8	6.7	5.9	6.7	
$\Delta S^{\ddagger}$	−19.1	−34.6	−24.2	−28.2	−30.1	
$\Delta G^{\ddagger}_{298}$	16.7	16.1	13.9	14.3	15.7	

[a]Units: temperature (K), rate constants (M^{-1} min^{-1}), rates (M min^{-1}), energies (kcal mol^{-1}), entropies (cal mol^{-1} K^{-1}). Keq is an equilibrium constant defined by equation (1) and was determined experimentally at different temperatures. [b]Rates of the reaction at 7 min of reaction time were calculated using the following concentrations of the reagents that were determined from experimental and simulated reaction profiles: [Fe_aH] = 1.00×10^{-5} M, [Fe_a] = 1.00×10^{-5} M, [acetone] = 0.15 M, [1-phenethanol] = 0.15 M, [acetophenone] = 0.262 M, [*i*PrOH] = 12.4 M, temperature 301 K.

dx.doi.org/10.1021/ja304814s | *J. Am. Chem. Soc.* 2012, 134, 12266−12280

Scheme 4. Synthesis of Complex 4

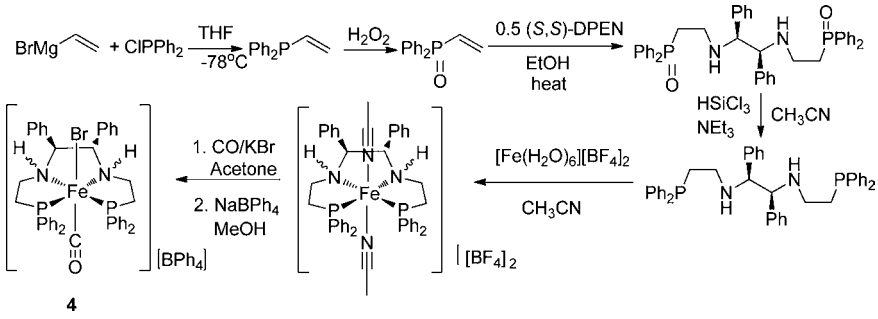

isotope effect (KIE_2 = 1.3) was detected when *i*PrOD-d_1 was used. The different intercepts of the rate lines on the time axis show that the activation period is longer when *i*PrOD-d_8 is used compared with the reactions involving *i*PrOD-d_1 and *i*PrOH. These observations indicate that the transfer of the hydridic hydrogen of isopropanol, as opposed to the hydroxyl hydrogen, dominates the rate of activation of the precatalyst and that a hydride transfer likely also dominates the rate of catalyst turnover. More data will be needed in order the separate the relative contributions of these processes to the KIE values.

The Preparation and Reactivity of 4 Containing a Diamine Ligand. The complex **4** that contains a P-NH-NH-P ligand with amine groups instead of imines can be synthesized as described in Scheme 4. It was fully characterized using spectroscopic methods. Single crystals of **4** were analyzed by X-ray diffraction (Figure 12). The monocationic complex **4** has a distorted octahedral geometry with carbonyl and bromide ligands trans to each other. The phenyl groups of the diamine are in equatorial positions and the amine hydrogens are axial, anti with respect to each other. The bond lengths between ligand donor atoms and the iron are within the expected range.[16] A wide P−Fe−P angle (107.99(7)°) results from the structure of the ligand, which forms three five-membered ligand−metal rings. This is comparable to P−Fe−P angles observed for similar iron complexes prepared in our laboratory.[16]

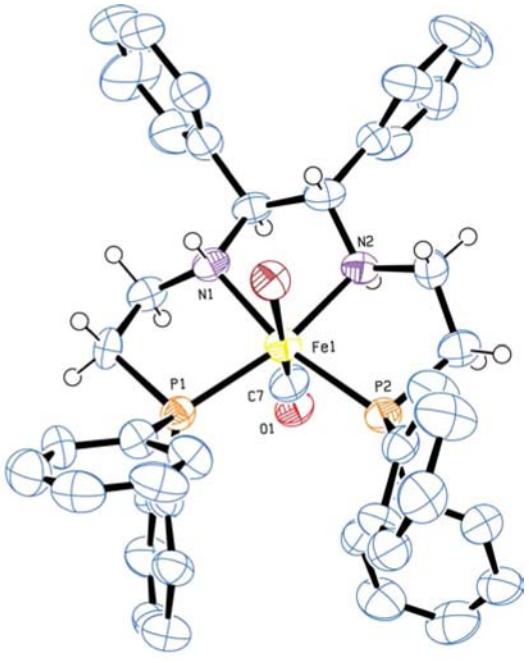

Figure 12. ORTEP plot of the cation of **4**. Thermal ellipsoids are drawn at 50% probability. Some hydrogen atoms, solvent molecules, and counterions are omitted for clarity. Selected interatomic distances [Å] and angles [deg]: N1−Fe1 2.065(5), P1−Fe1 2.259(2), C7−Fe1 1.745(9), Br1−Fe1 2.490(1), P1−Fe1−P2 107.99(7).

The reduction of acetophenone using complex **4** was performed under standard conditions that were used for the kinetic studies of complex **2**. After 2 h of reaction only 10% of the ketone was converted to the corresponding alcohol with an enantiomeric excess of 82% (*R*).

Preparation and Properties of the Ene−Amido Complex 5. Complex **2** was reacted with 2.5 equivalents of the base KO*t*Bu in benzene at room temperature to produce a green solid after purification. The ^{1}H NMR spectra of the product in benzene-d_6 shows that the resonances corresponding to the hydrogen atoms of the complex **2** are absent but a new set of multiplets was observed. These peaks were assigned to the hydrogens H_a', H_d', H_e' and H_h' of the neutral bis(ene−amido) iron complex **5** (Figure 13). Coupling between H_a'-H_c' and H_f'-H_h' were identified using 2D COSY experiments to locate the resonances of H_c' and H_f' that were overlapping with aromatic peaks. An absence of the resonances arising from tetraphenylborate in the ^{11}B NMR spectrum and in the aromatic region of ^{1}H NMR spectra peaks is consistent with the formulation of **5** as a neutral complex. This highly soluble complex gave an AB pattern in the ^{31}P{^{1}H} NMR spectrum at 68.9 and 68.6 ppm with $^2J_{PP}$ = 25 Hz, which is consistent with a structure having two inequivalent phosphorus atoms. The reaction of the complex **5** with a 1 M solution of HCl in diethyl ether (excess was added) resulted in the formation of complex **6**, the structure of which was confirmed by ^{31}P{^{1}H} NMR (two doublets at 64.9 and 67.0 ppm, $^2J_{PP}$ = 40.4 Hz) and HRMS ESI$^+$ (full monocation of the complex **6**). This reversibility of the reaction of the precatalyst **2** with base and acid further supports the structure of the complex **5**.

The stability of complex **5** was lower than that of the bis(ene-amido) complex **3** (Figure 1) as expected since precatalyst **2** when activated with base produces a far more reactive catalytic solution than **3**. The decomposition of compound **5** in solution or in the solid state under an inert atmosphere occurred after days but after seconds in the air. Decomposition in solution is signaled by a broadening of the peaks in the ^{1}H NMR spectra, resulting from the formation of paramagnetic species, and by a change of color from a deep green to a brown-green. This high reactivity prevented the full characterization of this compound using elemental analysis, high resolution mass spectroscopy or X-ray diffraction.

Compound **5** was directly reacted with a mixture of acetophenone in *i*PrOH (standard conditions applied) without

dx.doi.org/10.1021/ja304814s | J. Am. Chem. Soc. 2012, 134, 12266−12280

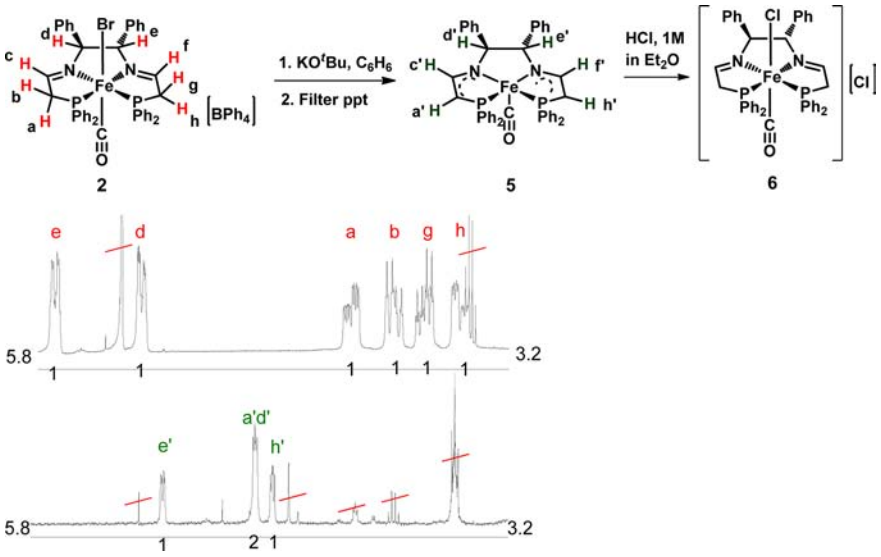

Figure 13. Formation of the bis(ene−amido) complex **5** and the comparison of a selected region (3.2−5.8 ppm) of the ^{1}H NMR spectrum of the complexes **2** in CD_2Cl_2 and **5** in C_6D_6.

the addition of base to test whether it is within the catalytic cycle. The observed reaction profile in terms of the formation of 1-phenethanol with time is presented in Figure 14, run 1.

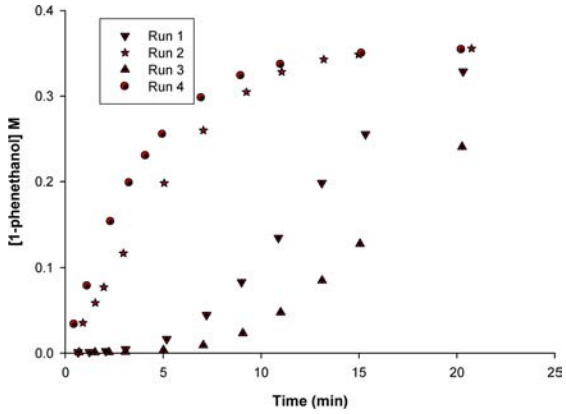

Figure 14. Catalytic reduction of acetophenone using complex **5**. Run 1: complex **5** reacted with a solution of acetophenone in *i*PrOH. Run 2: complex **5** reacted with *i*PrOH for 4 min prior to the addition of acetophenone. Run 3: complex **5** reacted with acetophenone for 4 min prior to the addition of *i*PrOH. Run 4: complex **5** was reacted with *i*PrOH for 12 min prior to the addition of acetophenone.

The reactivity and enantioselectivity of the complex **5** in the process of acetophenone reduction are comparable to those observed with complex **2** activated by base. On the other hand, the apparent activation period indicates that complex **5** needs to be activated prior to the catalytic cycle to take place; thus, it is not within the catalytic cycle.

Since the reaction of complex **5** with *i*PrOH and acetophenone led to the formation of the active catalyst (Figure 14, run 1), it can be concluded that one of these reagents is responsible for the activation of **5**. Each was reacted with the complex **5** for 4 min prior to the addition of the other in order to identify, which of the two substances is an activating agent (Figure 14, runs 2 and 3, respectively). The induction period disappeared when **5** was prereacted with *i*PrOH (run 2) but was very pronounced when acetophenone was reacted with **5** before *i*PrOH was added (run 3). These observations show that the activation of the green complex **5** results from its reaction with *i*PrOH. The longer induction period of run 3 relative to that of run 1 (Figure 14) is consistent with the finding of the kinetic study that the enolate of acetophenone prolongs the period of activation of the catalyst. The kinetic studies also predict that the formation of the active species in the solution is a continuous process that takes place during the entire acetophenone reduction step of the reaction. This implies that the concentration of the active catalytic species and the rate of 1-phenethanol formation will be greater if the preactivation of the green compound **5** with *i*PrOH is allowed to occur for a longer period of time, keeping other conditions the same. The reaction where **5** is preactivated with *i*PrOH for 12 min (Figure 14, run 4) verifies that this is the case.

Protonation of the Active Catalytic Species and Synthesis of Complex 7. In order to gain information about the structures of the catalytically active complexes, *i*PrOH was added to the complex **5**. The green solution turned an orange-red color after 20 min. The ^{31}P{^{1}H} NMR spectrum of the reaction mixture showed a complicated pattern of broad resonances, indicating that several species were formed. These species might be Fe_A, Fe_AH, **5**, and decomposition products. The isolation and characterization of the observed complexes is difficult due to their high reactivity. On the other hand, when the reaction was quenched with a 1 M solution of HCl in diethyl ether (excess was added), the solution became bright yellow. The solvent was evaporated to give a yellow solid. The major species in the ^{31}P{^{1}H} NMR spectrum of the solid dissolved in CD_2Cl_2 had two doublet resonances at 56.2 and 66.0 ppm with J_{P-P} = 39.3 Hz (~85% relative to all the species that produced ^{31}P resonances). The solid was purified by precipitation with $NaBPh_4$ from MeOH solution and identified as the amine−imine complex **7** (Scheme 5) on the basis of HRMS ESI$^+$, ^{1}H and ^{31}P{^{1}H} NMR spectroscopy. The structure of complex **7** is similar to the structure of complex **6** except that one of the imine functionalities of the ligand is reduced to the amine. The reduction possibly occurred via selective transfer of the hydride from *i*-PrO$^-$ to one of the imines of the ligand as described in Scheme 5. It also has to be

dx.doi.org/10.1021/ja304814s | J. Am. Chem. Soc. 2012, 134, 12266−12280

Scheme 5. Proposed Formation of the Complex 7

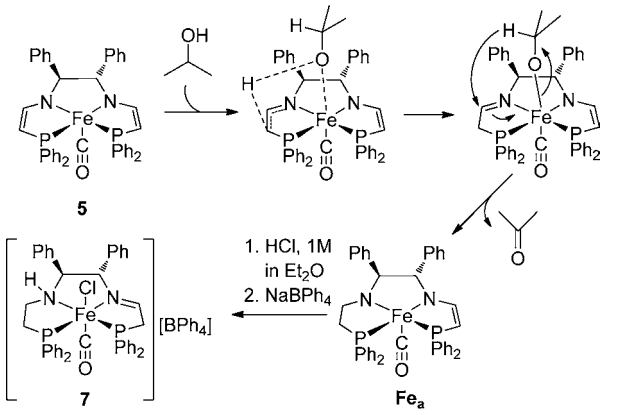

noted that only one diastereomer of complex 7 was observed (two possible diastereomers may arise from reduction of one or the other imine of the ligand), since only two doublets were observed in ^{31}P $\{^1H\}$NMR spectra, indicating that the reaction is stereospecific.

Catalytic Activity of Complex 7. The use of complex 7 as a catalyst precursor under the standard conditions results in the rapid catalytic reduction of acetophenone without an induction period (Figure 15; see the Supporting Information for the conditions). The TOF is 55,000 h^{-1} at 25% conversion compared to 28,000 h^{-1} using complex **2** under standard conditions. The ee of the 1-phenylethanol produced in each case was 82% (*R*).

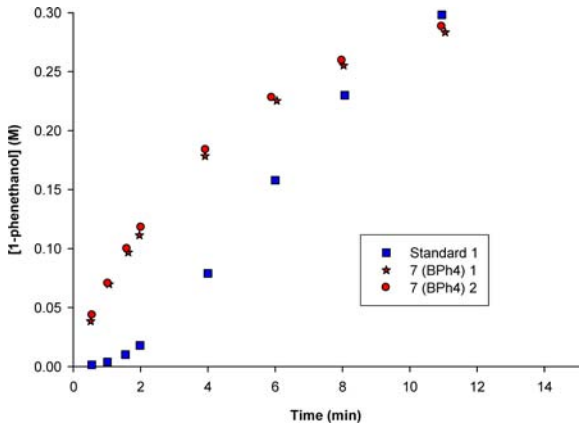

Figure 15. Reaction profiles of catalytic reduction of acetophenone using complexes **2** (standard run) and 7 (duplicate runs).

DISCUSSION

The presence of the activation period prior the catalytic cycle of the reaction makes it difficult to use conventional techniques to determine the rates of individual steps of the reaction, since it is impossible to enforce the conditions such that the active catalyst would be at steady-state. Hartmann and Chen have used an alternative approach, which was initially outlined by Boudart, to investigate the catalytic cycle of asymmetric transfer hydrogenation of Noyori's precatalyst $RuCl_2$(diamine)-(diphosphine).[32] The approach is based on utilization of coupled differential rate laws of individual steps of the process, which arise directly from the proposed mechanistic model, in numerical integrations. If these numerical integrations are fitted to the experimentally obtained reaction profiles, then the rate constants and rates of the individual steps of the process can be determined.

In order to propose the kinetic model, we established the dependences of the rates of activation of the catalyst and 1-phenethanol formation on concentrations of the reagents. The mechanistic model (Scheme 2 and Scheme 3) was used to derive coupled differential rate laws (eq 7, eq (S18)-eq (S28)), for elementary steps of the catalytic process. The extent of 1-phenethanol production with time was simulated using these rate laws. The simulated reaction profiles, which were obtained using the rate constants summarized in Table 1, are in good agreement with the data obtained experimentally (Figure 8). This implies that the proposed model effectively describes the catalytic process. Simulations were also used to show that the formation of the active species is a prolonged process (Figure 8, E). It suggests that the activation is a complex process involving major changes in the structure of the complex going from the precatalyst to the catalyst. A similar approach was used to determine the activation parameters of individual steps of the reaction from the reaction profiles that were obtained by conducting the catalytic reductions at different temperatures.

A logical explanation for the activation period is that the imine groups are reduced to amines to produce an iron complex with hydride and amine groups to allow the hydride-protic amine outer sphere reduction of the ketone that is observed for PNNP ruthenium catalysts. Complex **4**, which contains a ligand with two amine groups, is a significantly less active precatalyst compared the complex **2**. This indicates that the complete reduction of the ligand does not lead to the formation of the active catalyst. The enantiomeric excess of the 1-phenethanol produced using **4** as a precatalyst is identical to that using complex **2**. This may be explained by the fact that both **2** and **4** upon activation give the same active species, but complex **2** is activated faster to provide more of the active catalyst for the reaction. A complete reduction of the ligand from imine to amine may in fact be one of the possible catalyst deactivation pathways. Indeed deactivation is especially pronounced when the concentration of the substrate is low, but the concentration of isopropoxide is high.

The reaction of complex **2** with KO*t*Bu in nonprotic and nonreducing benzene as a solvent led to the formation of the bis(ene-amido) complex **5**. This reaction can be reversed if a strong acid such as HCl is added to the solution to give the chloro-carbonyl complex **6** containing the PNNP ligand identical to that of the complex **2**. It is evident that complex **5** is only an intermediate in the process of the catalyst activation since the induction period is still observed when **5** is reacted with a mixture of *i*PrOH and acetophenone to start the catalysis (Figure 14, run 1). The active catalyst is actually formed by the reaction of the complex **5** and *i*PrOH; thus when **5** is preactivated with *i*PrOH and then acetophenone is added (Figure 14, run 2), the reaction proceeds without an induction period.

The structures of the catalytically active species that form during the course of the reaction of **5** with *i*PrOH are very difficult to identify or isolate due to their high reactivity. They have been indirectly identified by quenching the catalyst solution with HCl and isolating complex 7 in good yield. Complex 7 has a PNNP ligand with both amine and imine functionalities. This strongly suggests that under the basic conditions of reaction the catalyst has a ligand with an ene-amido structure on one side and a saturated amido structure on

dx.doi.org/10.1021/ja304814s | J. Am. Chem. Soc. 2012, 134, 12266−12280

the other side (complex $\mathbf{Fe_a}$). Indeed, when complex **7** is treated with base under standard catalytic conditions, there is rapid catalysis without an induction period.

The above findings lead us to propose a mechanism involving the precatalyst activation as depicted in Scheme 6,

Scheme 6. Proposed Mechanism of Activation of the Precatalyst 2 to the Active Catalyst $\mathbf{Fe_a}$; Species 5 and $\mathbf{Fe_p}$ May Have Coordinated Isopropanol

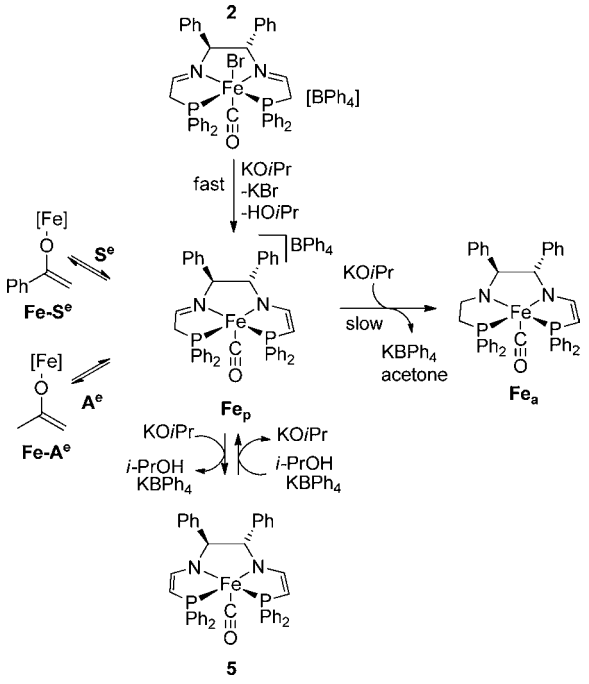

and the catalytic cycle as presented in Scheme 7. The activation is initiated by the fast reaction of complex **2** with the base to give $\mathbf{Fe_p}$. The slow step in the activation process is the reaction of $\mathbf{Fe_p}$ with $i\mathrm{PrO}^-$ to give $\mathbf{Fe_a}$. The equilibria involving $\mathbf{Fe_p}$ and the enolates of acetophenone and acetone (in later stage of the reaction) establish and interfere with the activation step. A second equivalent of base can react with $\mathbf{Fe_p}$ to give the doubly deprotonated complex **5**. We have not been able to obtain a clean sample or spectra of $\mathbf{Fe_p}$ to date, but **5** has been characterized. In the catalytic cycle, the activated catalyst $\mathbf{Fe_a}$ reacts with *i*PrOH (Scheme 7), presumably in an outer-sphere fashion, to give acetone and an iron hydride complex ($\mathbf{Fe_aH}$) which contains an H^-/H^+ pair with the hydride bound to the iron and proton to the nitrogen. The subsequent reaction of the $\mathbf{Fe_aH}$ with acetophenone produces 1-phenethanol and regenerates the complex $\mathbf{Fe_a}$.

Scheme 7. Proposed Mechanism of the Transfer Hydrogenation of Acetophenone

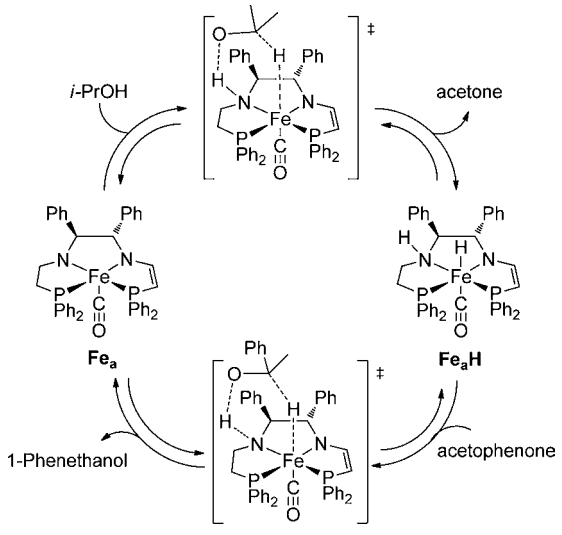

In the investigation of ketone reduction reactions using $RuCl_2(PPh_3)_3$[33] Backvall and co-workers proposed that the hydride transfer to the ketone occurs via its coordination to the metal followed by the insertion into the metal–hydride bond to give the alkoxide intermediate.[34] This mechanism, as well as the Meerwein–Ponndorf–Verley mechanism, which involves a direct transfer of the hydride between ketone and alkoxide when they are simultaneously coordinated to the metal,[35] are less likely to be operational in the catalytic system under investigation, since both of them require two or more vacant coordination sites. The outer-sphere mechanism that involves metal–ligand cooperation in transferring of the hydrogen equivalent is more probable. The mechanism involving a concerted hydride/proton transfer (H^-/H^+) from the metal and nitrogen to the carbon and oxygen of the ketone, respectively, was originally proposed by Noyori and co-workers[36] and is operational in many highly active catalytic reductions. A stepwise outer-sphere transfer of the hydrogen molecule (SWTH) is also known. In this mechanism the ketone is activated and oriented by noncovalent interaction with NH group of the ligand for the following attack of the metal-hydride. If the acidity of the ligand's amine group is low then the formation of the NH/alkoxide pair after the hydride transfer would be more favorable compared to the formation of alcohol/amido that is expected in a concerted outer-sphere mechanism. This mechanism was recently proposed by Baratta for a Ru(C-N-N)(P-P)Cl/base system[37] and by Bergens for a *trans*-$Ru(P\text{-}P)(H_2N\text{-}NH_2)(H)_2$ system.[7e] Gusev and co-workers were able to characterize in the solid state a ruthenium-secondary alkoxide complex also containing a P-N(H)-P and a carbonyl ligand; in solution this dissociates into a ruthenium hydride and ketone.[38]

It is a challenging task to differentiate between the concerted and stepwise outer-sphere mechanisms. The Baratta[39] and Bergens[7e] groups directly observed the metal-alkoxide intermediate. Baratta and co-workers also investigated the effect of the base that is present in the solution during transfer hydrogenation on the alkoxide/NH_2 intermediate. They suggested that *i*PrOH is competing with the $i\mathrm{PrO}^-$ for coordination to the NH_2–Ru complex; high base concentration favors the formation of the active alkoxide/NH_2 complex thus, increasing the rate of the catalytic reduction of ketones. Our iron system showed no dependence on the base concentration when the ratio of base to **2** was greater than 5:1. It was also shown that the decrease in rate of 1-penethanol formation when the ratio of the base to **2** is smaller than 5:1 resulted from the slower rate of activation of the catalyst and not from a slower rate of the catalytic reduction process. Complex **5**, without the addition of any base, can be activated by *i*PrOH to produce a highly active catalyst (Figure 15). In addition, the activation entropy value for the hydride transfer step reported by Baratta et al. (−3.2 eu)[38] in the system operating via a ruthenium-alkoxide/amine intermediate is less negative than the activation entropy observed for our system (−28.6 eu for

dx.doi.org/10.1021/ja304814s | J. Am. Chem. Soc. 2012, 134, 12266–12280

the k_2 step, Table 2). Thus a bimolecular attack of an iron hydride on the ketone is more consistent with this value than an intramolecular reaction involving an iron alkoxide complex.[35b,40,41]

The secondary amido nitrogen of complex $\mathbf{Fe_a}$ is expected to be highly basic. The adjacent ene−amido part of the ligand makes this amido nitrogen even more basic. Therefore, it is reasonable to assume that complex $\mathbf{Fe_a}$, when exposed to an excess of protic solvent such as *i*PrOH, would be protonated at the amido nitrogen and give a coordinatively unsaturated monocationic iron complex. Accordingly the process of hydride transfer would be a more difficult step than the transfer of the proton and this would explain why there is a small KIE for the transfer of the proton but a significant KIE for the transfer of the hydride. The observed KIE of 2.5 is comparable to other KIE measured for HM-NH vs DM-ND attack on ketones.[44] Casey and Johnson concluded in a detailed study of Noyori's transfer hydrogenation catalyst that both the observed isotope effects of 1.79 for transfer of OH to nitrogen and of 2.86 for transfer of CH to ruthenium from isopropanol are much too large to be equilibrium isotope effects. They argued for a concerted transfer of the hydride and proton.[41] We propose that the transfer of a proton from *i*PrOH to the amido complex is a fast process followed by a slower transfer of the hydride. Similarly the transfer of the hydride from iron(II) to the acetophenone is the slowest step. This explains why the rate of catalytic reduction is sensitive to the nature of the ketone that is used.[14]

With only a cursory glance at the activation parameters of Table 2, one might think that the k_1 step, the formation of the iron-hydride, should be rate determining since it has a greater free energy of activation. However, under experimental conditions where the concentration of *i*PrOH is significantly higher than the concentration of acetophenone, the slowest rate of the process is the hydride transfer from $\mathbf{Fe_aH}$ to the ketone. The evidence for $\mathbf{Fe_aH}$ and $\mathbf{Fe_a}$ comes from the HCl quenching reaction and DFT calculations, as described elsewhere.[45]

CONCLUSIONS

The current study provides evidence that the activation of precatalyst **2** with base results in the selective reduction of one of the imine groups of the starting P−N−N−P ligand to give a highly active catalyst $\mathbf{Fe_a}$ for the enantioselective transfer hydrogenation of acetophenone. This catalyst likely contains a P−N−N−P ligand with amido and ene−amido functionalities. Only the presence of both functionalities in the structure results in high catalytic activity; the bis(amine) complex **4**, and the bis(ene-amido) complex **5** require activation. The proposed structure of the amido(ene−amido) catalyst $\mathbf{Fe_a}$ is supported by its reaction with acid to give complex **7** that contains a PNNP ligand with an amine and imine functionality. Precatalyst **7** under our mild standard conditions leads to the most active catalyst known for the asymmetric reduction of acetophenone and does not require an observable activation period before highest rate of the catalysis is achieved.

The determined activation parameters suggest that the catalytic reduction of acetophenone occurs via an outer-sphere mechanism. The determined KIE for the transfer of the hydride to the carbonyl carbon indicates that the rate-determining step may not involve a concerted hydride/proton transfer but rather a stepwise hydride addition and then proton transfer mechanism. The kinetics studies provided rate constants for the proposed mechanism. DFT results that support the proposed mechanism over alternatives are in hand and will be published in the near future.[45]

EXPERIMENTAL SECTION

General Procedure for the Reduction of Acetophenone Using Iron-Based Precatalysts 2, 4, and 7. The stock solutions were prepared in a glovebox according to the details provided in the Supporting Information. The stock solution 1 (**SS1**) was prepared by dissolving the precatalyst in acetophenone. The stock solution 2 (**SS2**) was prepared by dissolving KO^{t}Bu in *i*PrOH. These solutions were used only after all the solids were completely dissolved and for less than two days. A required mass of the **SS1** was added to a vial containing *i*PrOH charged with a stirring bar and acetophenone to form mixture 1 (**M1**). A required mass of **SS2** was added to a second vial containing *i*PrOH to give mixture 2 (**M2**). In order to ensure a constant temperature of the experiment inside a glovebox, **M1** and **M2** were placed into a sand bath with a coil connected to the Fisher Scientific temperature control unit for 15 min. To initiate the reaction, **M1** and **M2** were efficiently mixed by transferring the solutions from vial to vial and placed into a sand bath attached to the stirring plate. The final concentrations of the reagents were adjusted to be as follows [acetophenone] = 0.412 M, [**2**], [**4**], or [**7**] = 6.73×10^{-5} M, [KO*t*Bu] = 5.45×10^{-4} M and [*i*PrOH] = 12.4 M (standard conditions). The samples were taken by injecting small portions of the reaction mixture into septa-sealed GC vials containing aerated *i*PrOH for efficient quenching of the reaction. Samples were analyzed using a Perkin-Elmer Autosystem XL chromatograph with a chiral column (CP chirasil-Dex CB 25 m × 2.5 mm). Hydrogen gas was used as a mobile phase at a column pressure of 5 psi. The injector temperature was 250 °C, and the FID temperature was 275 °C. The amount of 1-phenethanol in the sample was determined relative to the amount of the acetophenone. The retention times of acetophenone, 1-phenethanol (*R*), and 1-phenethanol (*S*) were found to be 5.02, 8.73, and 9.42 min, respectively, if the temperature of the oven was kept at 130 °C.

Synthesis of Complex [Fe(CO)(Br)(Ph$_2$PCH$_2$CH$_2$-N(H)-((*S*,*S*)-CH(Ph)CH(Ph)-N(H)-CH$_2$CH$_2$-PPh$_2$][BPh$_4$] (4). The procedures for the synthesis of the ligand precursors (diphenylvinyl phosphine and diphenylvinyl phosphine oxide) and for the preparation and reduction of O═P-N-N-P═O were adopted with modifications from work of Rahman et al.[42] and Cook et al.[43] and are presented in the Supporting Information. The P-N-N-P ligand (*S*,*S*)-1,2-diphenyl-ethylamine-*N*,*N*′-bis-diphenylethylphosphine (0.260 g, 0.410 mmol) was dissolved in 15 mL of acetonitrile in 20 mL vial charged with a stirring bar. Hexaquairon tetrafluoroborate (0.138 g, 0.410 mmol) was added dropwise to the reaction mixture as a solution in acetonitrile (3 mL) to give an instantaneous change in color from colorless to deep purple. After 3 h the solvent was removed from the reaction mixture to give a deep, purple solid that was mixed with potassium bromide (0.073 g, 0.61 mmol) and redissolved in acetone (15 mL) and placed under atmosphere of carbon monoxide (1.1 atm) and stirred overnight at 38 °C to give a yellow solution with a white precipitate that was filtered through Celite. Solvent was removed under vacuum to give a yellow solid that was redissolved in methanol (10 mL). A solution of NaBPh$_4$ (0.14 g, 0.41 mmol) in 3 mL of methanol was added dropwise to give an instantaneous formation of the yellow precipitate. The precipitate was filtered and washed with methanol (3 × 1 mL), dried, and washed with diethyl ether (3 × 2 mL) to give complex **4** as a yellow-orange solid (0.093 g, 20% yield). Crystals suitable for the X-ray analysis were obtained by the diffusion of diethyl ether into solution of **4** in dichloromethane and methanol mixture. ^{1}H NMR (400 MHz, CD_2Cl_2) δ: 2.19−2.40 (m, 1H, PCH*H*), 2.45−2.64 (m, 1H, PCH*H*), 2.76−2.97 (m, 1H, PCH*H*, 1H, NCH*H*), 3.04−3.33 (m, 1H, PCH*H*, 1H, NCH*H*, 1H, NCH*H*), 3.62−3.86 (m, 1H, NCH*H*, 1H, N*H*), 4.15−4.30 (m, 1H, NC(Ph)*H*), 4.48−4.62 (m, 1H, NC(Ph)*H*), 5.05−5.20 (m, 1H, N*H*), 6.75−7.60 (m, 50H, Ar*H*); ^{13}C{^{1}H} NMR (100 MHz; CD_2Cl_2) δ: 33.24−33.62 (m, PCH_2), 34.78−33.62 (m, PCH_2), 46.21 (s, NCH_2), 50.69 (s, NCH_2), 71.08 (s, NC(Ph)H), 75.28 (s, NC(Ph)H), 121.6 (s, BPh), 125.5−125.6 (m, BPh), 128.9−

dx.doi.org/10.1021/ja304814s | J. Am. Chem. Soc. 2012, 134, 12266−12280

135.6 (m, ArCH), 135.0−135.9 (m, BPh), 163.9 (m, J_{CB} = 49.3 Hz, BPh), 216.6 (m, CO); $^{31}P\{^{1}H\}$ NMR (161 MHz; CD_2Cl_2): 55.18 (d, J_{PP} = 39.3 Hz), 58.03 (d, J_{PP} = 39.3 Hz); HRMS (ESI-TOF) m/z calculated for $[C_{43}H_{42}N_2P_2FeOBr]^+$: 799.1299, found: 799.1315. Anal. Calcd for $C_{67}H_{62}N_2P_2FeBrOB$: C, 71.87; H, 5.58; N, 2.5. Found: C, 71.52; H, 6.25; N, 2.58.

Synthesis of Complex Fe(CO)(Ph_2PCH═CHN-((*S*,*S*)-CH(Ph)-CH(Ph))-N-CH═$CHPPh_2$) (5). In an argon glovebox a solution of KO^{t}Bu (sublimed, 0.013 g, 0.112 mmol) in 5 mL of benzene was added to a vial charged with a stirring bar containing complex **2** (0.050 g, 0.044 mmol). The solution instantaneously became green and a white precipitate was observed. The reaction mixture was stirred for an additional 10 min, filtered through the glass-frit and the solvent was evaporated from the resulting green solution to give a bright green powder. The powder was redissolved in 5 mL of hexanes upon the addition of a few drops of benzene. This solution was filtered through the Celite, and the solvent was evaporated. Yield: 0.019 g, 59.3%. ^{1}H NMR (400 MHz, C_6D_6) δ: 4.49−4.57 (m, 1H, PC*H*), 4.59−4.68 (m, 1H, PC*H*, 1H, NC(Ph)*H*), 5.06−5.16 (m, 1H, NC(Ph)*H*), 6.94−7.50 (m, 30H, Ar*H*), 7.31−7.51 (m, 2H, NC*H*); $^{31}P\{H\}$ NMR (161 MHz; C_6D_6) δ: 68.9 (d), 68.6 (d) ppm $^2J_{PP}$ = 25 Hz.

Synthesis of Complex [Fe(CO)(Cl)($Ph_2PCH_2CH_2N$(H)-((*S*,*S*)-CH(Ph)CH(Ph))-N═$CHCH_2PPh_2$)][BPh_4] (7). *i*PrOH (3 mL) was cooled to −25° in a freezer in an argon glovebox and added to a vial charged with stirring bar containing complex **5** (0.014 g, 0.020 mmol). The reaction mixture was stirred and allowed to warm up to 25 °C. A gradual change of color of the solution was observed from green to orange-red over the course of 25 min of the reaction. The reaction was quenched with a 1 M solution of HCl in diethyl ether (excess added), which instantaneously gave a yellow solution. The solvent was evaporated from the reaction mixture to a give yellow solid as a product. The $^{31}P\{^{1}H\}$ NMR spectrum of the crude product in CD_2Cl_2 showed that the major product had doublet resonances at 55.15 and 64.92 ppm with J_{PP} = 39.4 Hz, which accounted for more than 85% of the material present. The compound was further purified. The crude product was dissolved in 1 mL of methanol followed by the addition of a solution (1 mL) of $NaBPh_4$ (0.013 g, 0.038 mmol) in methanol. The product was isolated as a yellow solid (yield: 0.011 g, 53%). ^{1}H NMR (500 MHz, CD_2Cl_2) δ: 2.61−2.77 (m, 2H, NCH_2), 3.09−3.33 (m, 2H, PCH_2 amine side), 3.81−3.95 (m, 2H, PCH_2 imine side), 4.38−4.49 (m, 1H, C(Ph)*H* amine side), 4.57−4.69 (m, 1H, N*H*), 4.93−5.02 (m, 1H, C(Ph)*H* imine side), 7.70−7.82 (m, 1H, N═C*H*), 6.84−7.67 (m, 50H, Ar*H*); $^{13}C\{^{1}H\}$ NMR (100 MHz; CD_2Cl_2) δ: 46.72−47.11 (m, PCH_2), 49.46 (s, $HNCH_2$), 49.51−49.92 (m, PCH_2), 76.50 (s, NC(Ph)H), 77.69 (s, NC(Ph)H), 121.3 (s, BPh), 124.-125.1 (m, BPh), 129.9−135.6 (m, ArCH), 135.2−136.2 (m, BPh), 163.7 (m, J_{CB} = 49.3 Hz, BPh), the resonances for the carbonyl (CO) and imine (N═C) carbons were not detected in the spectra due to their longer relaxation times compared to the other carbons in the structure and the lower intensity of the signal due to the expected multiple splitting by ^{31}P nuclei; $^{31}P\{H\}$ NMR (161 MHz; CD_2Cl_2): 55.15 (d, J_{PP} = 39.4 Hz), 64.92 (d, J_{PP} = 39.4 Hz); HRMS (ESI-TOF) m/z calculated for $[C_{43}H_{40}N_2P_2FeOCl]^+$: 753.1648, found: 753.1637.

General Procedure for the Reduction of Acetophenone Using Complex 5. In an argon glovebox complex **5** (0.019 g, 0.027 mmol) was dissolved in benzene (2.00 g). The resulting green, clear solution (0.050 g) was added to vials charged with stirring bars. The benzene was evaporated to give solid samples of complex **5** (0.48 mg, 0.000665 mmol) in the vials. These were used in reduction reactions with acetophenone and *i*PrOH. **Run 1**: A solution of acetophenone (0.476 g, 3.96 mmol) in *i*PrOH (7.192 g) was prepared in an argon glovebox and the temperature of the solution equilibrated to 28 °C. The solution was added to the vial with complex **5** to initiate the reaction. The reaction progress was monitored by taking samples of the reaction mixture and quenching them by injection into aerated *i*PrOH in a sealed GC vial. **Run 2**: The solvent *i*PrOH (7.192 g) was thermostatted at 28 °C and added to the vial containing complex **5** and stirred for 4 min. Acetophenone (0.476 g, 3.96 mmol) was added to the reaction mixture to initiate the reaction. The reaction progress was monitored in a similar fashion as in run 1. **Run 3**: Acetophenone (0.476 g, 3.96 mmol) was thermostatted at 28 °C and added to the vial containing complex **5** and stirred for 4 min. Isopropanol (7.192 g) was added to the reaction mixture to initiate the reaction. The reaction progress was monitored in a similar fashion as in run 1. **Run 4**: Same as run 2, but the activation reaction with *i*PrOH was left for 12.4 min before adding the substrate.

■ ASSOCIATED CONTENT

Ⓢ Supporting Information

General experimental procedures, exact initial concentrations used in kinetic experiments, rate determination plots, and rate law derivation; X-ray crystallographic data in CIF format for complex **4**. This material is available free of charge via the Internet at http://pubs.acs.org.

■ AUTHOR INFORMATION

Corresponding Author

rmorris@chem.utoronto.ca

Notes

The authors declare no competing financial interest.

■ ACKNOWLEDGMENTS

R.H.M. thanks NSERC for a Discovery grant. We thank Dr. Shun Lo for assistance with the rate law simulation program and Ben Thomas for preliminary work on the chemistry of Scheme 4. A.A.M. was supported by an Ontario Graduate Scholarship (OGS).

■ REFERENCES

(1) (a) de Vries, J. G., Elsevier, C. J., Eds. *Handbook of Homogeneous Hydrogenation*; Wiley-VCH: Weinheim, Germany, 2007; Vol. 3, pp 1131−1163. (b) Minnaard, A. J.; Feringa, B. L.; Lefort, L.; de Vries, J. G. *Acc. Chem. Res.* **2007**, *40*, 1267−1277. (c) Malacea, R.; Poli, R.; Manoury, E. *Coord. Chem. Rev.* **2010**, *254*, 729−752. (d) Ikariya, T.; Blacker, A. J. *Acc. Chem. Res.* **2007**, *40*, 1300−1308. (e) Genet, J. P. *Acc. Chem. Res.* **2003**, *36*, 908−918. (f) Noyori, R.; Ohkuma, T. *Angew. Chem., Int. Ed.* **2001**, *40*, 40−73. (g) Andersson, P. G., Munslow, I. J., Eds. *Modern Reduction Methods*; Wiley-VCH: Weinheim, Germany, 2008.

(2) (a) Ringenberg, M. R.; Ward, T. R. *Chem. Commun.* **2011**, *47*, 8470−8476. (b) Bogar, K.; Martin-Matute, B.; Backvall, J. E. *Beilstein J. Org. Chem.* **2007**, *3*, 50−53. (c) Servi, S.; Tessaro, D.; Pedrocchi-Fantoni, G. *Coord. Chem. Rev.* **2008**, *252*, 715−726. (d) Matsuda, T.; Yamanaka, R.; Nakamura, K. *Tetrahedron: Asymmetry* **2009**, *20*, 513−557.

(3) (a) Kagan, H. B., Ed. *Organocatalytic Enantioselective Reduction of Olefins, Ketones, and Imines*; Wiley-VCH: New York, 2007. (b) Li, D.; He, A. Y.; Falck, J. R. *Org. Lett.* **2010**, *12*, 1756−1759.

(4) (a) Chase, P. A.; Jurca, T.; Stephan, D. W. *Chem. Commun.* **2008**, 1701−1703. (b) Chase, P. A.; Welch, G. C.; Jurca, T.; Stephan, D. W. *Angew. Chem., Int. Ed.* **2007**, *46*, 8050−8053. (c) Stephan, D. W.; Erker, G. *Angew. Chem., Int. Ed.* **2009**, *49*, 46−76.

(5) (a) Blaser, H. U.; Malan, C.; Pugin, B.; Spindler, F.; Steiner, H.; Studer, M. *Adv. Synth. Catal.* **2003**, *345*, 103−151. (b) Naud, F.; Spindler, F.; Rueggeberg, C. J.; Schmidt, A. T.; Blaser, H. U. *Org. Process Res. Dev.* **2007**, *11*, 519−523. (c) Blaser, H. U., Federsel, H. J., Eds. *Asymmetric Catalysis on Industrial Scale: Challenges, Approaches and Solutions*; Wiley-VCH: Weinheim, Germany, 2010.

(6) (a) Hedberg, C. Gladiali, S.; Taras, R. In *Modern Reduction Methods*; Andersson, P. G., Munslow, I. J., Eds.; Wiley-VCH: Weinheim, Germany, 2008: Chapters 5−6, pp 109−152. (b) Bullock, R. M. *Chem.—Eur. J.* **2004**, *10*, 2366−2374. (c) Johnson, N. B.; Lennon, I. C.; Moran, P. H.; Ramsden, J. A. *Acc. Chem. Res.* **2007**, *40*, 1291−1299.

(7) For recent reviews see: (a) Clapham, S. E.; Hadzovic, A.; Morris, R. H. *Coord. Chem. Rev.* **2004**, *248*, 2201−2237. (b) Samec, J. S. M.;

Backvall, J. E.; Andersson, P. G.; Brandt, P. *Chem. Soc. Rev.* **2006**, *35*, 237−248. (c) Sandoval, C. A.; Bie, F. S.; Matsuoka, A.; Yamaguchi, Y.; Naka, H.; Li, Y. H.; Kato, K.; Utsumi, N.; Tsutsumi, K.; Ohkuma, T.; Murata, K.; Noyori, R. *Chem.—Asian J.* **2010**, *5*, 806−816. (d) Soni, R.; Cheung, F. K.; Clarkson, G. C.; Martins, J. E. D.; Graham, M. A.; Wills, M. *Org. Biomol. Chem.* **2011**, *9*, 3290−3294. (e) Takebayashi, S.; Dabral, N.; Miskolzie, M.; Bergens, S. H. *J. Am. Chem. Soc.* **2011**, *133*, 9666−9669.

(8) For recent reviews see: (a) Junge, K.; Schroder, K.; Beller, M. *Chem. Commun.* **2011**, *47*, 4849−4859. (b) Morris, R. H. *Chem. Soc. Rev.* **2009**, *38*, 2282−2291. (c) Bauer, G.; Kirchner, K. A. *Angew. Chem., Int. Ed.* **2011**, *50*, 5798−5800. (d) Mancheno, O. G. *Angew. Chem., Int. Ed.* **2011**, *50*, 2216−2218.

(9) (a) Casey, C. P.; Guan, H. R. *J. Am. Chem. Soc.* **2007**, *129*, 5816−5817. (b) Sui-Seng, C.; Freutel, F.; Lough, A. J.; Morris, R. H. *Angew. Chem., Int. Ed.* **2008**, *47*, 940−943. (c) Langer, R.; Leitus, G.; Ben-David, Y.; Milstein, D. *Angew. Chem., Int. Ed.* **2011**, *50*, 2120−2124.

(10) For recent examples see: (a) Enthaler, S.; Erre, G.; Tse, M. K.; Junge, K.; Beller, M. *Tetrahedron Lett.* **2006**, *47*, 8095−8099. (b) Enthaler, S.; Hagemann, B.; Erre, G.; Junge, K.; Beller, M. *Chem.—Asian J.* **2006**, *1*, 598−604. (c) Furuta, A.; Nishiyama, H. *Tetrahedron Lett.* **2008**, *49*, 110−113. (d) Buchard, A.; Heuclin, H.; Auffrant, A.; Le Goff, X. F.; Le Floch, P. *Dalton Trans.* **2009**, 1659−1667. (e) Naik, A.; Maji, T.; Reiser, O. *Chem. Commun.* **2010**, *46*, 4475−4477. (f) Kandepi, V.; Cardoso, J. M. S.; Peris, E.; Royo, B. *Organometallics* **2010**, *29*, 2777−2782.

(11) Zhou, S. L.; Fleischer, S.; Junge, K.; Das, S.; Addis, D.; Beller, M. *Angew. Chem., Int. Ed.* **2010**, *49*, 8121−8125.

(12) (a) Casey, C. P.; Guan, H. R. *J. Am. Chem. Soc.* **2009**, *131*, 2499−2507. (b) Chen, H. Y. T.; di Tommaso, D.; Hogarth, G.; Catlow, C. R. A. *Dalton Trans.* **2011**, *40*, 402−412. (c) Chakraborty, S.; Guan, H. R. *Dalton Trans.* **2010**, *39*, 7427−7436.

(13) (a) Meyer, N.; Lough, A. J.; Morris, R. H. *Chem.—Eur. J.* **2009**, *15*, 5605−5610. (b) Sonnenberg, J.; Coombs, N.; Dube, P. A.; Morris, R. H. *J. Am. Chem. Soc.* **2012**, *134*, 5893−5899.

(14) Mikhailine, A.; Lough, A. J.; Morris, R. H. *J. Am. Chem. Soc.* **2009**, *131*, 1394−1396.

(15) (a) Mikhailine, A. A.; Kim, E.; Dingels, C.; Lough, A. J.; Morris, R. H. *Inorg. Chem.* **2008**, *47*, 6587−6589. (b) Mikhailine, A. A.; Lagaditis, P. O.; Sues, P. E.; Lough, A. J.; Morris, R. H. *J. Organomet. Chem.* **2010**, *695*, 1824−1830.

(16) (a) Lagaditis, P. O.; Lough, A. J.; Morris, R. H. *Inorg. Chem.* **2010**, *49*, 10057−10066. (b) Sues, P. E.; Lough, A. J.; Morris, R. H. *Organometallics* **2011**, *30*, 4418−4431.

(17) Mikhailine, A. A.; Morris, R. H. *Inorg. Chem.* **2010**, *49*, 11039−11044.

(18) Lagaditis, P. O.; Lough, A. J.; Morris, R. H. *J. Am. Chem. Soc.* **2011**, *133*, 9662−9665.

(19) (a) Mezzetti, A. *Dalton Trans.* **2010**, *39*, 7851−7869. (b) Bonaccorsi, C.; Mezzetti, A. *Curr. Org. Chem.* **2006**, *10*, 225−240.

(20) (a) Gao, J. X.; Ikariya, T.; Noyori, R. *Organometallics* **1996**, *15*, 1087−1089. (b) Gao, J. X.; Yi, X. D.; Xu, P. P.; Tang, C. L.; Wan, H. L.; Ikariya, T. *J. Organomet. Chem.* **1999**, *592*, 290−295. (c) Rautenstrauch, V.; Hoang-Cong, X.; Churlaud, R.; Abdur-Rashid, K.; Morris, R. H. *Chem.—Eur. J.* **2003**, *9*, 4954−4967. (d) Li, T. S.; Churlaud, R.; Lough, A. J.; Abdur-Rashid, K.; Morris, R. H. *Organometallics* **2004**, *23*, 6239−6247.

(21) Spogliarich, R.; Kaspar, J.; Graziani, M. *J. Organomet. Chem.* **1986**, *306*, 407−412.

(22) Carrion, M. C.; Sepulveda, F.; Jalon, F. A.; Manzano, B. R.; Rodriguez, A. M. *Organometallics* **2009**, *28*, 3822−3833.

(23) Hagen, C. M.; Vieille-Petit, L.; Laurenczy, G.; Suss-Fink, G.; Finke, R. G. *Organometallics* **2005**, *24*, 1819−1831.

(24) Watzky, M. A.; Finke, R. G. *J. Am. Chem. Soc.* **1997**, *119*, 10382−10400.

(25) Widegren, J. A.; Finke, R. G. *J. Mol. Catal. A: Chem.* **2003**, *198*, 317−341.

(26) Whitesides, G. M.; Hackett, M.; Brainard, R. L.; Lavalleye, J.; Sowinski, A. F.; Izumi, A. N.; Moore, S. S.; Brown, D. W.; Staudt, E. M. *Organometallics* **1985**, *4*, 1819−1830.

(27) Jaska, C. A.; Manners, I. *J. Am. Chem. Soc.* **2004**, *126*, 9776−9785.

(28) (a) Anton, D. R.; Crabtree, R. H. *Organometallics* **1983**, *2*, 855−859. (b) Eberhard, M. R. *Org. Lett.* **2004**, *6*, 2125−2128.

(29) Hornstein, B. J.; Aiken, J. D.; Finke, R. G. *Inorg. Chem.* **2002**, *41*, 1625−1638.

(30) Bordwell, F. G. *Acc. Chem. Res.* **1988**, *21*, 456−463.

(31) Wettergren, J.; Buitrago, E.; Ryberg, P.; Adolfsson, H. *Chem.—Eur. J.* **2009**, *15*, 5709−5718.

(32) Hartmann, R.; Chen, P. *Adv. Synth. Catal.* **2003**, *345*, 1353−1359.

(33) Aranyos, A.; Csjernyik, G.; Szabo, K. J.; Backvall, J. E. *Chem. Commun.* **1999**, 351−352.

(34) (a) Pamies, O.; Backvall, J. E. *Chem.—Eur. J.* **2001**, *7*, 5052−5058. (b) Fulton, J. R.; Holland, A. W.; Fox, D. J.; Bergman, R. G. *Acc. Chem. Res.* **2002**, *35*, 44−56.

(35) (a) Degraauw, C. F.; Peters, J. A.; Vanbekkum, H.; Huskens, J. *Synthesis* **1994**, 1007−1017. (b) Cohen, R.; Graves, C. R.; Nguyen, S. B. T.; Martin, J. M. L.; Ratner, M. A. *J. Am. Chem. Soc.* **2004**, *126*, 14796−14803.

(36) (a) Takehara, J.; Hashiguchi, S.; Fujii, A.; Inoue, S.; Ikariya, T.; Noyori, R. *Chem. Commun.* **1996**, 233−234. (b) Haack, K. J.; Hashiguchi, S.; Fujii, A.; Ikariya, T.; Noyori, R. *Angew. Chem., Int. Ed.* **1997**, *36*, 285−288.

(37) (a) Baratta, W.; Chelucci, G.; Gladiali, S.; Siega, K.; Toniutti, M.; Zanette, M.; Zangrando, E.; Rigo, P. *Angew. Chem., Int. Ed.* **2005**, *44*, 6214−6219. (b) Baratta, W.; Bosco, M.; Chelucci, G.; Del Zotto, A.; Siega, K.; Toniutti, M.; Zangrando, E.; Rigo, P. *Organometallics* **2006**, *25*, 4611−4620.

(38) (a) Bertoli, M.; Choualeb, A.; Lough, A. J.; Moore, B.; Spasyuk, D.; Gusev, D. G. *Organometallics* **2011**, *30*, 3479−3482. (b) Bertoli, M.; Chouale, A.; Gusev, D. G.; Lough, A. J.; Major, Q.; Moore, B. *Dalton Trans.* **2011**, *40*, 8941−8949. (c) Clarke, Z. E.; Maragh, P. T.; Dasgupta, T. P.; Gusev, D. G.; Lough, A. J.; Abdur-Rashid, K. *Organometallics* **2006**, *25*, 4113−4117.

(39) Baratta, W.; Siega, K.; Rigo, P. *Chem.—Eur. J.* **2007**, *13*, 7479−7486.

(40) Kuo, L. Y.; Finigan, D. M.; Tadros, N. N. *Organometallics* **2003**, *22*, 2422−2425.

(41) Casey, C. P.; Johnson, J. B. *J. Org. Chem.* **2003**, *68*, 1998−2001.

(42) Rahman, M. S.; Oliana, M.; Hii, K. K. *Tetrahedron: Asymmetry* **2004**, *15*, 1835−1840.

(43) Cook, V. C.; Willis, A. C.; Zank, J.; Wild, S. B. *Inorg. Chem.* **2002**, *41*, 1897−1906.

(44) Gomez-Gallego, M.; Sierra, M. A. *Chem. Rev.* **2011**, *111*, 4857−4963.

(45) Prokopchuk, D. E.; Morris R. H. Submitted.